

86

LBNL-40840
UC-412



ERNEST ORLANDO LAWRENCE BERKELEY NATIONAL LABORATORY

The Discovery of High-Redshift Supernovae and Their Cosmological Implications

Alex G. Kim
Physics Division

September 1997
Ph.D. Thesis

RECEIVED
NOV 06 1997
OSTI

MASTER

19980528 085

DISTRIBUTION OF THIS DOCUMENT IS UNLIMITED

DTIC QUALITY INSPECTED 1

ja

DISCLAIMER

This document was prepared as an account of work sponsored by the United States Government. While this document is believed to contain correct information, neither the United States Government nor any agency thereof, nor The Regents of the University of California, nor any of their employees, makes any warranty, express or implied, or assumes any legal responsibility for the accuracy, completeness, or usefulness of any information, apparatus, product, or process disclosed, or represents that its use would not infringe privately owned rights. Reference herein to any specific commercial product, process, or service by its trade name, trademark, manufacturer, or otherwise, does not necessarily constitute or imply its endorsement, recommendation, or favoring by the United States Government or any agency thereof, or The Regents of the University of California. The views and opinions of authors expressed herein do not necessarily state or reflect those of the United States Government or any agency thereof, or The Regents of the University of California.

Ernest Orlando Lawrence Berkeley National Laboratory
is an equal opportunity employer.

LBNL-40840
UC-412

**The Discovery of High-Redshift Supernovae
and Their Cosmological Implications**

Alex G. Kim
Ph.D. Thesis

Department of Physics
University of California, Berkeley

and

Physics Division
Ernest Orlando Lawrence Berkeley National Laboratory
University of California
Berkeley, CA 94720

September 1997

**The Discovery of High-Redshift Supernovae and
Their Cosmological Implications**

by

Alex G. Kim

B.S. (University of Michigan at Ann Arbor) 1991

M.A. (University of California at Berkeley) 1994

A dissertation submitted in partial satisfaction of the
requirements for the degree of

Doctor of Philosophy

in

Physics

in the

GRADUATE DIVISION

of the

UNIVERSITY of CALIFORNIA at BERKELEY

Committee in charge:

Professor Marc Davis, Chair
Professor Richard Muller
Doctor Saul Perlmutter
Professor Alexei Filippenko

1996

Contents

List of Figures	v
List of Tables	vii
1 Introduction	1
2 Photometry	6
2.1 Introduction	6
2.2 Supernova Counts and Uncertainties	7
2.2.1 Galaxy Subtraction	9
2.2.2 Reference Count Error	12
2.2.3 New Image Count Error	14
2.2.4 Matching Count Error	14
2.3 Calibrations	16
2.4 Instrumental Corrections	18
3 K Corrections	28
3.1 Introduction	29
3.2 A Generalized K Correction	30
3.3 K_{xy} Calculation	31
3.4 Error Estimates and Determination of Optimal Filter Pair	33
3.5 Conclusions	39
4 Implications for the Hubble Constant from the First Seven Supernovae at $z \geq 0.35$	55
4.1 Introduction	56
4.2 The Distant Type Ia supernova Sample	59
4.3 The determination of H_0^L/H_0^G	59
4.4 The Hubble Constant	65
4.5 Conclusions	67

List of Figures

2.1	A representative image of a supernova field from the supernova search.	8
2.2	Images of the host galaxy, images of the combined supernova and galaxy, and images of the difference of the two for each of the seven supernovae.	10
2.3	Bessell's representation of the Cousins R band and the effective transmission of the INT R Mould filter with the EEV5 CCD.	19
2.4	Instrumental Corrections at $z = 0.374$ for INT images taken with the Mould filter and KP2m references.	23
2.5	Instrumental Corrections at $z = 0.374$ for INT images taken with the Harris filter and KP2m references.	24
2.6	Instrumental Corrections at $z = 0.42$ for INT images taken with the Mould filter and KP2m references.	25
2.7	Instrumental Corrections at $z = 0.42$ for INT images taken with the Harris filter and KP2m references.	26
3.1	Bessell's representations of the Johnson-Cousins B , V , and R passband transmission functions, S_B , S_V , and S_R . The dotted lines represent the "blueshifted" R transmission function, $S_R(\lambda(1+z))$, at $z = 0.2$ and at $z = 0.5$. These $S_R(\lambda(1+z))$ transmission functions roughly match the $S_V(\lambda)$ and $S_B(\lambda)$ transmission functions for these values of z	47
3.2	$K_{VR}(z = 0.5)$ as a function of epoch for SN 1981B, SN 1990N, and SN 1992A.	48
3.3	$K_{BR}(z = 0.5)$ as a function of epoch for SN 1981B, SN 1990N, and SN 1992A.	49
3.4	(a) $K_{RR}(z = 0.5)$ (or the R band K correction) as a function of epoch for SN 1981B and SN 1990N. The available spectra of SN 1992A do not have sufficient coverage to make such a calculation. (b) $K_{BR}(z = 0.5)$ from Figure 3 plotted on the same scale as (a) to show the much smaller range, due to the close match of the R filter at $z = 0.5$ with the B filter at rest.	50

3.5	Comparison between the Bessell representation of R and our constructed response of the KPNO R as described in the text, normalized at peak transmission.	51
3.6	$K_{BR}^{Bessell} - K_{BR}^{KPNO}$ as a function of observed color for all redshifts. . .	52
3.7	The root-mean-square scatter of K_{BR} (squares) and K_{VR} (stars) for SN 1992A at epochs -1 and 3 days after maximum, and SN 1981B at epoch 0 as a function of redshift.	53
3.8	$K_{BR} - K_{BR}^{counts}$ as a function of redshift for epochs $-14 \leq t_0^B \leq 76$ days after maximum.	54
4.1	The best fit H_0^L/H_0^G with 68% (short dashes) and 95% (dot-dashes) error range for each value of Ω_M in an (a) $\Lambda = 0$ universe and (b) flat universe, using the five light-curve corrected supernova magnitudes. (These are the results from a single parameter fit; the uncertainties are calculated for each value of Ω_M .)	69
4.2	The solid lines show contours of constant H_0^L/H_0^G and H_0^G when Ω_M and Ω_Λ are fixed. They are labeled with their value and associated uncertainties based on the five corrected supernova magnitudes. The values of H_0^L/H_0^G and H_0^G derived from the seven uncorrected supernova magnitudes are given in parentheses for the approximately corresponding contour.	70

List of Tables

3.1	Selected Spectra of Type Ia supernovae	41
3.2	K_{BR} for a range of redshifts. Ellipses (...) denote redshifts for which there is insufficient spectral coverage.	42
3.3	Table 3.2, continued.	43
3.4	K_{VR} for a range of redshifts. Ellipses (...) denote redshifts for which there is insufficient spectral coverage.	44
3.5	Table 3.4, continued.	45
3.6	K_{RR} for a range of redshifts. Ellipses (...) denote redshifts for which there is insufficient spectral coverage. Note that only a few available spectra have sufficient wavelength coverage to make any K_{RR} calculations.	46
4.1	Supernova Data and Photometry Error Budget	71
4.2	The 95% One-Tailed Confidence Levels for H_0^L/H_0^G	71

Acknowledgements

The success of the Supernova Cosmology Project has been the result of the combined effort of many people, without whom this dissertation would never have been realized. Their number is too many to list here, but they know who they are: the undergraduates, graduates, post-docs, scientists, visitors, collaborators, and fellow graduate students who have provided me with an exciting and fun scientific environment to work in. I would particularly like to thank all my office mates who have made every day an adventure.

I want to thank my three "advisors" who have shepherded me through graduate school and who have shown me the fun and excitement of science, and also the responsibilities of the scientist. Professor Richard Muller has proven how much more there is to physics than just physics; how an active and open mind with a good idea can produce excellent science from the most unexpected places. I have learned much from working with Professor Gerson Goldhaber "in the trenches". He has reminded me not to lose sight of my objectives, no matter how lost I got in their nitty-gritty details. He was also the one with whom I could kick back and down a beer with at the end of the day. I have the honor of being Dr. Saul Perlmutter's first thesis student. He has taught me more than I can enumerate. And I appreciate the cheerful way that he has done so, with an open door and a patience to listen to any nonsense I would have to say, ready to steer me to the right path.

I want to thank my parents, who have always let me free to choose my life paths.

I also thank my sister Michelle for being there.

I thank my other committee members, Professors Marc Davis and Alex Filippenko, for actually signing this dissertation.

Finally, I want to thank all the friends who have served to impede my educational progress during my 22 years of school. In particular, I thank those around me during the past five and a half years of graduate school. Without them I most certainly would have produced this dissertation much sooner, but we sure did have some fun!

Chapter 1

Introduction

Observations from the first half of this century of supernova peak magnitudes (Baade 1938), light-curve shapes (Wilson 1939), and spectra (Minkowski 1939) gave astronomers their first hint of the homogeneity of supernovae and their potential as a tool for studying cosmology. The eventual classification of Type Ia supernovae, supernovae whose spectra show silicon but lack hydrogen features (Minkowski 1939,1940; Elias et al. 1985; Branch 1986; Harkness et al. 1987; Porter & Filippenko 1987), has isolated a supernova subclass whose properties are remarkably similar. Type Ia supernovae are now thought to be the result of thermonuclear explosions triggered by accretion on a Carbon/Oxygen white dwarf (Nomoto, Thielemann, & Yokoi 1984). Such a system has a built-in fuse, the Chandrasekhar mass limit, which can naturally account for the homogeneity of these events.

Interest in Type Ia supernovae has led to careful studies that are now giving

us a new understanding of the family. Recent observations of variations in peak absolute magnitude, light-curve shape, spectral features, and colors indicate that Type Ia supernovae form a family, rather than a set of identical objects. However, these observables appear to be correlated with one another. Correlations between the light curve decay rate and peak absolute magnitude, examined for Type I by Pskovskii(1970, 1977) and further pursued by Phillips(1993), have led to the relations of Hamuy et al. (1995) and Riess, Press, & Kirshner(1995). Nugent et al. (1995) have shown that supernova magnitudes are related to relative spectral line strengths. The UV flux, as observed in $U - B$, also appears to be a good predictor of supernova brightness (Branch et al. 1996). These relations suggest that the Type Ia supernova family can be described by a single parameter, perhaps the mass of Ni^{56} produced during the explosion (Nugent et al. 1995).

Reaching a peak brightness of ~ -19 mag, Type Ia supernovae can equal and exceed the luminosity of their host galaxies and have been observed out to high redshift ($z \leq 0.85$) on optical 4-m class telescopes. They can also serve as distance indicators; despite the intrinsic variations in their peak magnitudes, each supernova transmits enough information to let us determine its intrinsic absolute magnitude and the amount of extinction the light has experienced getting to us.

Actually finding these potentially powerful tools for cosmology poses another problem. There are two main difficulties for supernova searching. Supernovae are rare, random events with roughly one visible supernova per galaxy every 500 years. They

are also quickly evolving objects which are brighter than $M_B^{max} + 2$ for only a month. Their window of time for detection is even shorter if they are to be discovered before maximum light. A search for distant supernovae was initiated by Nørgaard-Nielson et al. (1989) at the 1.5-m Danish telescope at La Silla, Chile. A probable Type II at $z = 0.28$ and a Type Ia at $z = 0.31$, SN1988U, were discovered from this effort. Unfortunately the supernovae were discovered more than a week past maximum light and were the only new discoveries from a couple of years of searching.

The Supernova Cosmology Project developed a new search strategy that ensured “on demand” supernovae discovered on the rising side of their light curves. Deep, wide-field R -band observations at the prime-focus of 2.5-m to 4-m telescopes are made of fields with known galaxy clusters or with little foreground pollution; each field contains hundreds of galaxies within the redshifts of interest. The same fields are imaged three weeks later (approximately two weeks in the supernova rest frame), a sufficiently short time to ensure that most of the new supernovae have not passed maximum light. These new images are searched for new point sources that were not visible or were much fainter in the earlier images. The discoveries are made within hours of the observation, triggering photometric and spectroscopic follow-up at previously coordinated and scheduled telescopes.

We have discovered 28 high-redshift supernovae in the redshift range 0.35 – 0.85; most have been confirmed to be Type Ia supernovae through spectra taken at the Keck telescope. Of these, the light curves of the first seven have been measured.

Several cosmological tests and measurements have been performed with this set. The apparent magnitudes of these high-redshift supernovae are used to simultaneously measure the mass density of the universe, Ω_M , and the normalized cosmological constant, $\Omega_\Lambda \equiv \Lambda/(3H_0^2)$, by examining their departure from a linear Hubble relation as predicted in the standard Friedmann-Lemaître cosmology. Since these supernovae are well into the cosmological flow, they also serve as a standard with which we can measure potential large-scale peculiar velocity flows that could affect local Hubble constant measurements. The light curves of the supernovae serve as clocks for a test of the cosmological time dilation expected in an expanding universe. Supernova rates at high redshifts have been measured, yielding not only information for galaxy evolution studies, but also clues to supernova progenitor systems.

In this thesis I discuss our methodology for doing photometry: from our procedure of extracting supernova counts from images that contain combined supernova plus galaxy flux, to our standard star calibration, to additional instrumental corrections that arise due to the multiple telescopes used for our observations. I discuss the different sources of photometric error and their correlations, and the construction of the covariance matrix for all the points in the light curve. I then describe the K corrections which account for the redshifting of spectra that are necessary to compare the photometry of our high-redshift data with those from nearby ($z \leq 0.1$) supernovae. Finally, I use the first seven of our supernovae to test the hypothesis that we live in an under-dense bubble where the locally measured Hubble constant differs significantly

from the true Hubble constant. I also use our data to place limits on the value of the Hubble constant. (Discussions of several other important aspects of our data analysis are or will be included in other papers. These topics include a description of how the covariance matrix is used to generate light-curve fits, a discussion of non-photometric systematic errors that also effect our measurements, and a discussion of the application of our supernovae to address other scientific/cosmological problems.)

Chapter 2

Photometry

2.1 Introduction

Our supernova data comes in the form of images taken at several different telescopes with Charge-Coupled-Device (CCD) detectors. Most of these images have field sizes of 15×15 arcmin² with plate scales of $0.3 - 0.5$ arcsec/pixel, depending on the specific telescope and detector used. A sample image is displayed in Figure 2.1. The first seven of our supernovae typically have data from nine nights distributed within a span of seventy days around the date of maximum light. Additional images were taken hundreds of days after the supernova discovery when the supernova light has presumably faded well beyond our detection thresholds. The bulk of the data was taken using an *R*-band filter and at least two images were taken per night. We construct from these data light curves, the supernova brightness in some standard

flux units as a function of time, for each of our supernovae.

There are several steps in producing the light curve. The first is to determine the number of CCD counts from each image that are from the supernova itself. The second step is to convert these counts into a standard flux system. The final step occurs because counts correspond to photo-electrons produced by photons that hit the CCD. A photon of fixed wavelength emitted by a supernova will have different probabilities of producing counts at different telescopes with different transmission efficiencies. We therefore apply a small “instrumental correction” that transforms the counts from all the images onto the same standard. In this chapter, I will describe both of these steps and the errors associated with each.

2.2 Supernova Counts and Uncertainties

The determination of supernova counts from our images is an involved process with several steps. The primary difficulty comes from the fact that the supernovae lie directly on top of their host galaxies, meaning that from the mixed galaxy + supernova counts, we have to “subtract” out the correct number of host galaxy counts to get the bare supernova counts. This is particularly difficult for high-redshift supernovae because their host galaxies have an angular area of only several seeing disks. (Seeing is here defined as the Full-Width-Half-Maximum of a point-source profile, given in angular units. A seeing disk is a disk with a diameter equal to the seeing.) This means that a significant amount of galaxy light will be mixed in with the super-

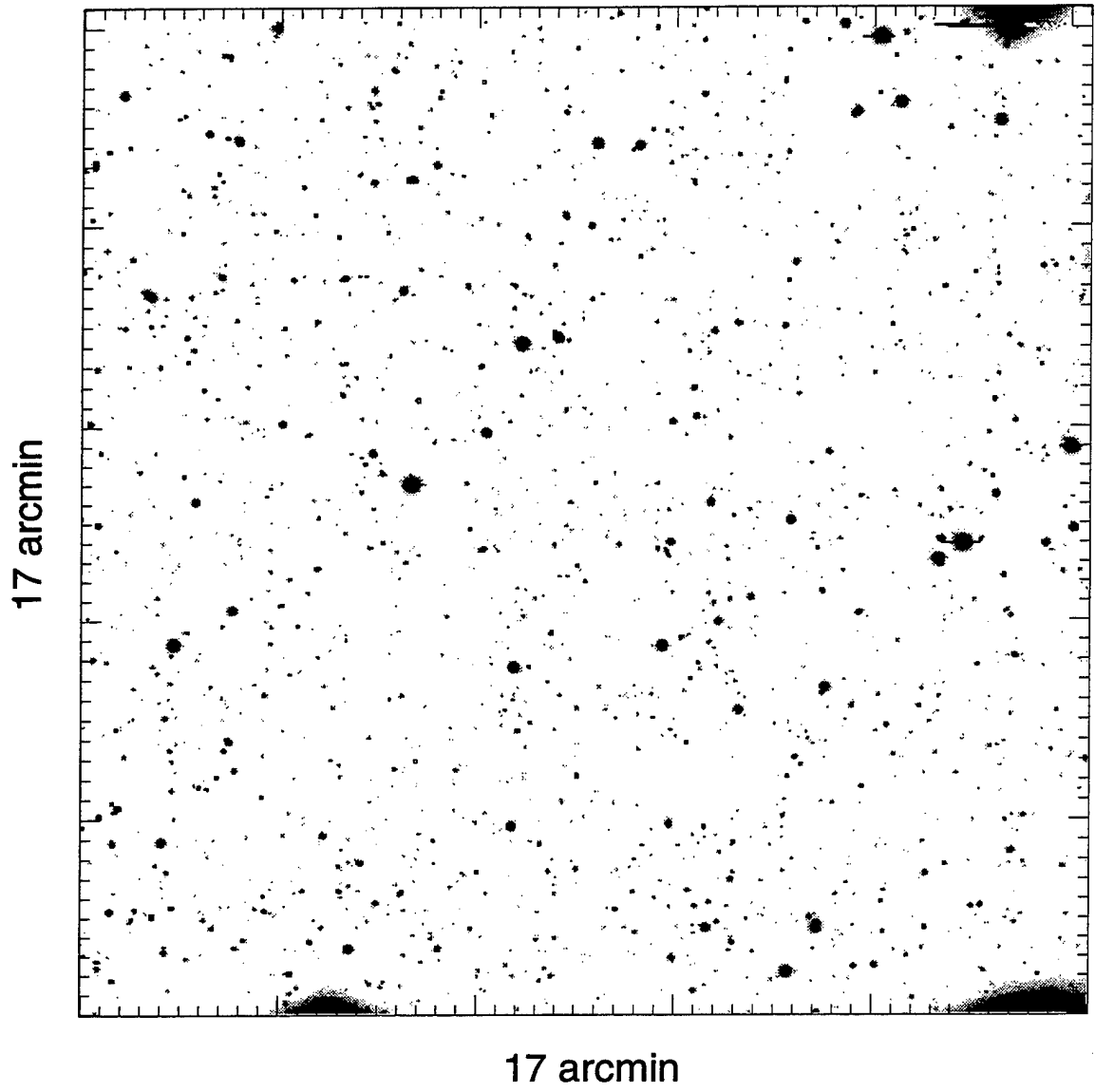


Figure 2.1: A representative image of a supernova field from the supernova search.

novae light. Figure 2.2 shows for each supernova, the image of the host galaxy, the galaxy+supernova image, and the difference between the two images. It is clear from these images that counts from the galaxy and counts from the supernova are mixed significantly.

Our basic strategy to measure the supernova counts is as follows. The number of galaxy counts at the supernova position is determined from a subset of images (called the “reference” images) taken when there should be little or no supernova signal. (We include the reference image counts when fitting the supernova peak magnitude in case there is some supernova signal in the references.) For each image, the total supernova + galaxy counts at the supernova position is subtracted by the galaxy counts, giving the supernova counts.

There are three main sources of uncertainty in our supernova counts. These are Poisson noise in the reference image, Poisson noise in the new image, and host galaxy subtraction matching errors due to uncertainties in ratios, point-spread-functions, and other sources described below.

2.2.1 Galaxy Subtraction

A subset of high signal-to-noise images with good seeing and little or no supernova signal are selected as “reference” images. The supernova counts from each image are determined from one-by-one comparisons (“subtractions”) with the galaxy counts from each of these reference images. A subtraction begins with the convolution of

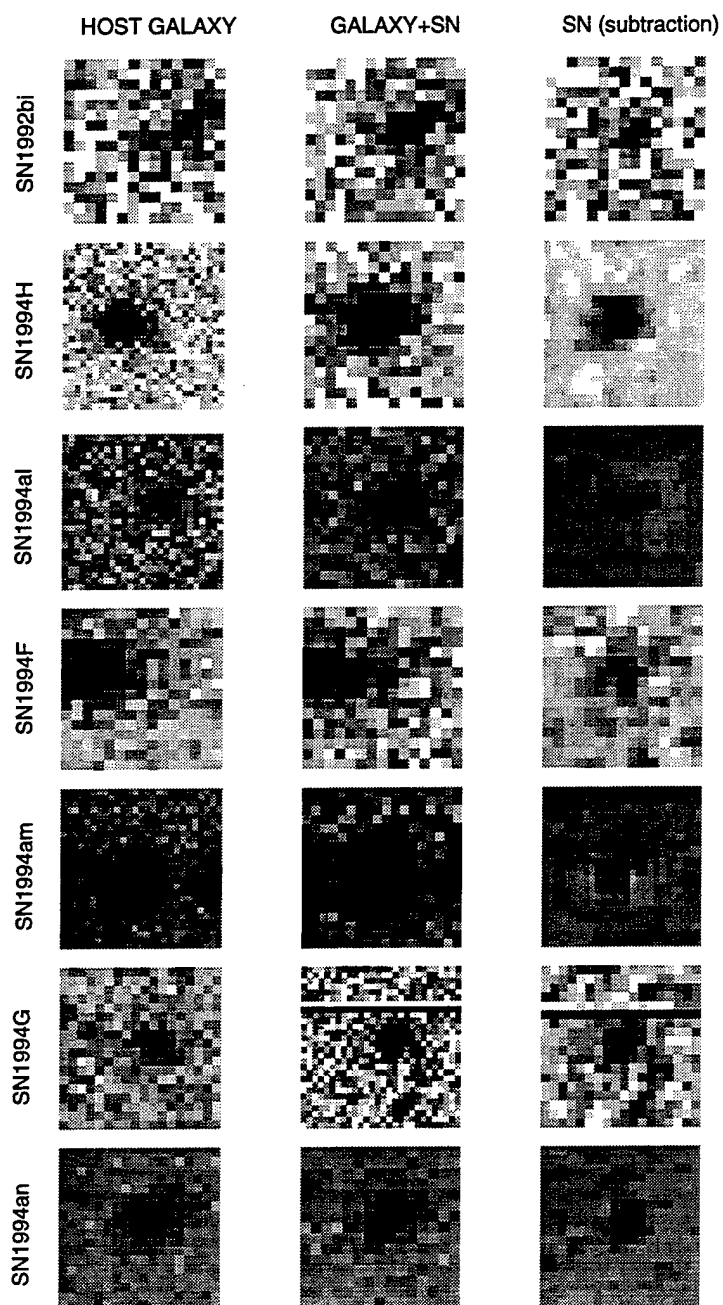


Figure 2.2: Images of the host galaxy, images of the combined supernova and galaxy, and images of the difference of the two for each of the seven supernovae.

the better seeing image to the point-spread-function of the broader seeing image. (The point-spread-functions are determined from fiducial stars located near the supernova.) Aperture counts are taken at the location of the supernova (calculated to high precision using the supernova signal from all the images) and on fiducial galaxies with similar observed $R - I$ colors as the host. Count ratios from these galactic fiducials normalize the image counts while ensuring that the host galaxy will be subtracted out. (This method is particularly important when matching images taken at different telescopes where the transmission efficiencies may differ slightly, resulting in color-dependent count ratios.) The difference between the normalized image and reference image counts at the supernova position is then renormalized to that of a “primary reference,” a single image to which all photometry in the light curve is normalized. The galaxy-subtracted supernova counts of a single image is then given by the weighted mean of the counts measured from subtractions between it and all the reference images.

To summarize, the galaxy subtracted number of counts from a single image is given by

$$f_i = \frac{\sum_{j=1}^{nref} \frac{1}{\sigma_{ij}^2} a_{ij} (n_{ij} - b_{ij} r_{ij})}{\sum_{j=1}^{nref} \frac{1}{\sigma_{ij}^2}}, \quad (2.1)$$

where n_{ij} are the counts in the new image i , and r_{ij} are the counts in the reference image j at the supernova position within one seeing disk, both after convolution and within apertures whose size depend on the point-spread-functions of the new image i and the reference image j . The ratio between the convolved images in fiducial galaxy

counts is given by b_{ij} , while a_{ij} represents the ratio between counts in the convolved new i image and the primary reference. The uncertainties from each subtraction is given by σ_{ij} . The uncertainty in counts for each point is

$$\sigma_i = \left(\sum_{j=1}^{nref} \frac{1}{\sigma_{ij}^2} \right)^{-\frac{1}{2}}. \quad (2.2)$$

There are alternatives to this method of determining the supernova counts. A subtraction image from the difference of the new and reference images could be produced and analyzed. Unfortunately, pixel resampling wreaks havoc with the point-spread-function, reducing the quality of convolutions and point-spread-function-weighted photometry. We have performed such subtractions on our images and they have provided us with a cross-check of our photometry. We are now considering a more innovative way to extract the light curve by fitting a constant background plus a point-spread-function of variable height located at the position of the supernova, simultaneously using all our images as input.

2.2.2 Reference Count Error

The underlying host galaxy counts from a set of reference images with high signal-to-noise ratios and good seeing are subtracted from measurements from all other images in order to give the light curve of the supernova alone. The reference counts have a sky dominated Poisson error which we have tried to minimize by selecting a deep set of reference images.

This reference error is correlated for all the points in the light curve. Each new image will have a different seeing and will thus require different amounts of underlying galaxy light to subtract out. The correlation in images for any two points will generally be the square of the Poisson error from the smaller of the two reference image apertures. Consider the reference image to consist of an area of a small seeing disk and successive annuli of increasing radii, r_{ann} . The correlated errors between two points on the light curve then come from regions of the reference image that are enclosed by the apertures used to measure both points. From Equation 2.1, we see that for each point, the uncertainty in the reference counts will contribute an error of

$$\frac{\sum_{j=1}^{nref} \frac{1}{\sigma_{ij}^2} a_{ij} b_{ij} (\sum_{r_{ann} < a_{per}} \sigma_{r_{ann}}^2)^{1/2}}{\sum_{j=1}^{nref} \frac{1}{\sigma_{ij}^2}}. \quad (2.3)$$

Thus, the off-diagonal terms in the covariance matrix, V , that describe the count errors of the points on the light curve are

$$V_{ij} = \frac{\sum_{k=1}^{nref} \frac{1}{\sigma_{ik}^2} a_{ik} b_{ik} (\sum_{r_{ann} < \min(a_{per_i}, a_{per_j})} \sigma_{r_{ann}}^2)^{1/2}}{\sum_{k=1}^{nref} \frac{1}{\sigma_{ik}^2}} \times \quad (2.4)$$

$$\frac{\sum_{l=1}^{nref} \frac{1}{\sigma_{jl}^2} a_{jl} b_{jl} (\sum_{r_{ann} < \min(a_{per_i}, a_{per_j})} \sigma_{r_{ann}}^2)^{1/2}}{\sum_{l=1}^{nref} \frac{1}{\sigma_{jl}^2}}. \quad (2.5)$$

Each reference image is also included in the light curve and is thus subtracted from the remaining set of reference images. The references are not assumed to be devoid of supernova light and are critical in fitting the zero level of the supernova counts. The columns and rows that correspond to reference images in the covariance matrix are calculated in a similar fashion as above, based on the partial derivatives of Equation 2.1, often producing negative terms (anti-correlations).

2.2.3 New Image Count Error

Generally, the largest source of count error for each photometric point comes from the Poisson noise of the new image. The sky background is the main contributor of this noise which is given as $\sigma_{new} = \left(\frac{\text{skycounts}}{\text{gain}}\right)^{1/2}$. This uncertainty is completely uncorrelated.

2.2.4 Matching Count Error

For each point on the light curve, the new or reference images are convolved to match point-spread-functions and the counts in a seeing disc from the new image is subtracted from the counts in the corresponding reference seeing disc. Ensuring proper matching requires determining the relative normalizations of the image counts, identifying the often spatially varying point-spread-functions, performing proper convolutions based on them (particularly difficult when comparing images of very different seeing), calculating the spatial transformations from image to image, and correctly handling resampling.

We test our matching for each individual photometry point by performing the subtraction analyses on a sample of fiducial objects in the same image which should give results of zero counts. The fiducials are selected based on a time series from all our images to ensure that they are not intrinsically variable objects within the time range of interest. We use objects that are similar in observed $R - I$ galaxy color and that are near the supernova within the image since some of our subtractions involve images

with spatially varying point-spread-functions from telescopes with slightly different transmission efficiencies. The fiducials are used to determine a matching error (which includes the reference-to-new count ratio error, the error in b_{ij}) by fitting σ_{match}^2 to $\frac{y_i}{(\sigma_{i_{stat}}^2 + \sigma_{match}^2)^{1/2}} - 1 = 0$, where y_i is the actual value of the subtraction and $\sigma_{i_{stat}}$ is the expected statistical error for the i 'th fiducial. If $\sigma_{match}^2 \approx 0$, then the full error can be accounted for by Poisson noise and the matching error is taken to be negligible. If the distribution is not normal or has $\sigma_{match}^2 > 0$, then there is significant matching error. As expected, there were no cases where $\sigma_{match}^2 \ll 0$.

We explored which images have large systematic errors and checked for correlations by examining all the subtractions for a set of fiducial objects with isophotal size similar to the host galaxy. Almost all subtractions with significant matching error involve particular telescopes or images with bad seeing. The Kitt Peak 4-m images (which had the largest variations in its point-spread-function within an image) and the Siding Spring Observatory images have larger than expected dispersions, although the images taken at these telescopes were taken under poor seeing conditions or poor transmission. Generally, there is appreciable σ_{match}^2 for images with seeing greater than 2.4 arcsec. For these images, there is no evidence for systematic trends for over- or under-subtraction, indicating that the larger convolutions contribute a significant random σ_{match}^2 that must be incorporated into our error budget.

2.3 Calibrations

Photometry is generally given in some standard system that describes energy flux, such as the Johnson-Cousins system, which is defined through a set of standard stars (groups of which lie in standard fields) and their tabulated, “true,” magnitudes (Johnson et al. 1953; Cousins 1976). (We use the secondary standard stars of Landolt 1992 and the tertiary standard stars of Davis 1995.) The instrumental (or observed) magnitudes ($-2.5 \log(\text{counts})$) of these standard stars will never exactly match their true magnitudes since the observing conditions that existed when the magnitudes of these stars were originally measured can never be exactly duplicated. Instrumental magnitudes must therefore be converted to the standard system based on the relationship between the observed and tabulated magnitudes of a set of standard stars. We parameterize the transformation between instrumental and true magnitudes with the coefficients a_0 (the magnitude zeropoint), a_1 (the color term), and a_2 (the airmass term), using the formula

$$R = -2.5 \log(\text{counts/sec}) + a_0 + a_1(V - R) + a_2\chi, \quad (2.6)$$

where χ is the airmass at which the image is taken and $(V - R)$ is the color of the star. (We have tried using both true and observed $(V - R)$ colors. Both give similar reduction in dispersion so we consistently use the true colors.) We find that second order terms do not significantly improve χ^2 per degree of freedom, nor do they visually appear to be important in our data. We thus do not include them in our fits.

Unlike with our supernova photometry where we measure counts within a seeing disk, we here use the number of counts within apertures with radii of several seeing lengths. In order to calibrate the supernova counts from the smaller aperture, we determine the ratio from integrating counts in large apertures and in a seeing disk for bright field stars in the image. (This final step is called the “aperture correction.”) An additional $2.5 \log(\text{ratio})$ is then added to the Equation 2.6 transformation.

Why do we use large aperture photometry to fit the transformation and a seeing disk to measure supernova counts? A larger aperture desensitizes the transformation on the exact shape of the point-spread-function and possible variations of the point-spread-function from image to image. The short exposure standard images often have different seeing conditions from the longer exposure images, and in one case the standard fields were deliberately defocused so the bright standards would not saturate the CCD. However, the use of a large aperture to measure a faint supernova would just add large amounts of sky noise to our photometry, whereas sky noise is negligible for the standard stars.

There are several tests that we perform on our data to check that the night was photometric, i.e., that the transmission efficiency remained constant throughout the night. As part of our search strategy, we take ~ 4 consecutive images of different fields and then go back to the same fields for second observations. This has the effect of placing a ~ 15 minute time gap between images of the same field, allowing us to reject asteroids and cosmic rays as candidates. This allows us to monitor the star

counts from each image pair to look for variations in transmission that could have occurred in the time between the two looks. The standard stars observed throughout the night are also used to check if the night was photometric. For the cases where our supernova and standard star images were taken through only a short portion of the night (images obtained by other observers, as a favor, or during engineering time), we performed similar tests of the transmission stability for the time spanning the observations. There still remain a few supernova fields for which the best calibration nights have questionable photometric conditions; for those cases we have assigned systematic errors based on the dispersion in star counts.

The errors on the fitted parameters result in errors of less than 0.01 mag. A much larger uncertainty comes from small variations in the transmission from image to image, generally on the order of ~ 0.02 mag. We include this transmission variability in our calibration error.

2.4 Instrumental Corrections

Placing supernovae (or any other object with a spectral-energy-distribution that is non-stellar) onto the Johnson-Cousins photometric system requires additional systematic photometry corrections. A standard star and supernova with the same color and identical observed magnitudes do not necessarily have the same standard magnitudes. Generally such corrections for Type Ia supernovae are negligibly small at early times in their evolution. However, if the observations are made with a non-standard

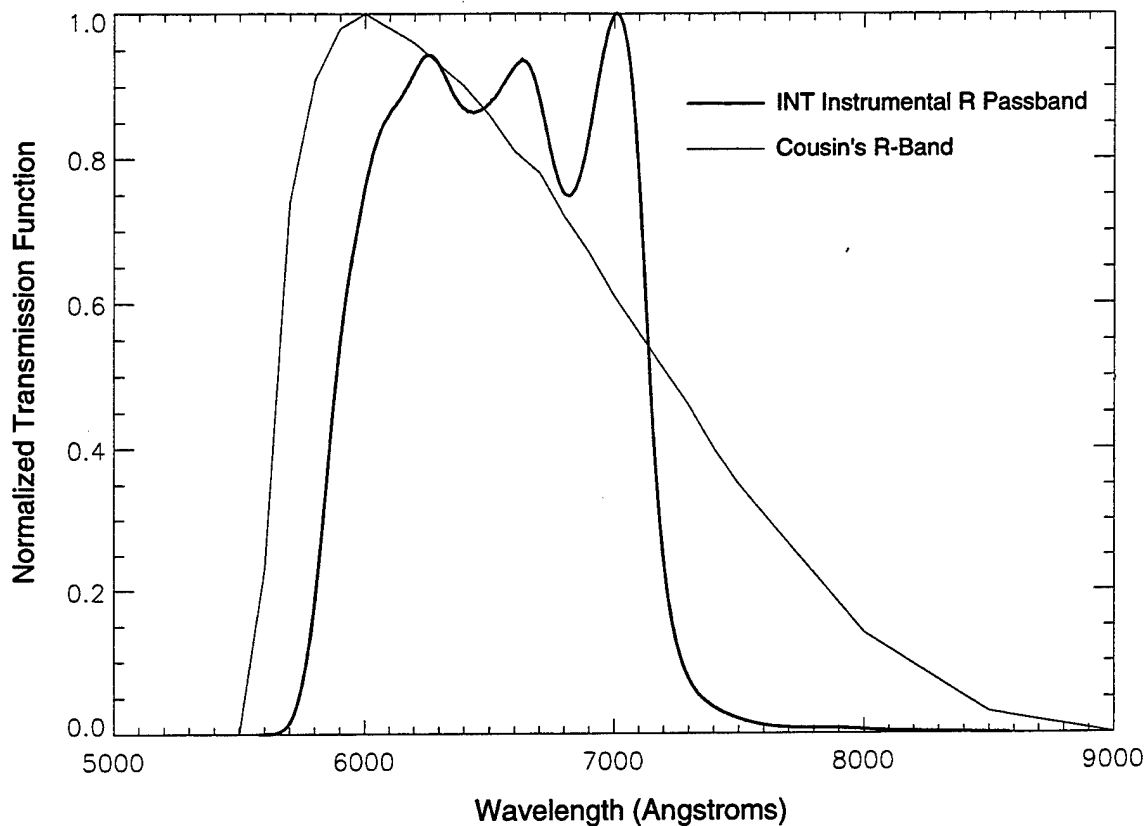


Figure 2.3: Bessell's representation of the Cousins R band and the effective transmission of the INT R Mould filter with the EEV5 CCD.

filter set or are of supernovae at certain redshifts and epochs, particular care must be taken if the magnitudes are to be used as a distance indicator. This effect is relevant to us because some of our data were taken with the Mould R filter which has a transmission as a function of wavelength that is narrower, redder, and flatter than standard R filters.

Another correction relevant to subtractions with images from different telescopes or instruments arises because galaxies with similar colors to the host galaxy are used to determine the ratio between counts in the new and reference images. The ratio

between galaxy counts are used in order to correctly subtract out the host galaxy light. However, that ratio would be different if the count ratio could be determined by a set of fiducial supernovae at the same redshift and epoch as our candidate. Supernovae and galaxies have contrasting spectral characteristics that will scale differently when observed through different transmission systems. Thus if we were to normalize the supernova counts using a galaxy ratio, we would be improperly scaling the supernova counts.

We present the process mathematically explicitly. Suppose we are trying to determine the Johnson-Cousins standard magnitude of a supernova with certain color and spectral energy distribution $SN(\lambda)$ based on our observed galaxy-subtracted magnitude. We can represent the Johnson-Cousins system by the transmission efficiencies produced by Bessell (1990), $F_{J-C}(\lambda)$, which have been designed so that their convolutions with standard star spectra reproduce their tabulated magnitudes. We denote by $S(\lambda)$ the spectrum of a standard star with the same $V - R$ color as our supernova. The host galaxy spectrum is given by $G(\lambda)$, and our reference and new images were taken with transmission efficiencies $F_R(\lambda)$ and $F_N(\lambda)$ respectively. What we measure as the instrumental magnitude from the analysis described above, m'_I , are the new counts (with galaxy and supernova counts) multiplied by a ratio determined using galaxies from which we subtract the reference signal:

$$m'_I = -2.5 \log \left(\frac{\int F_R(\lambda)G(\lambda)d\lambda}{\int F_N(\lambda)G(\lambda)d\lambda} \int F_N(\lambda) (SN(\lambda) + G(\lambda)) d\lambda - \int F_R(\lambda)G(\lambda)d\lambda \right). \quad (2.7)$$

If we didn't have to worry about subtracting the host galaxy, we would have observed

$$m_I = -2.5 \log \left(\int F_R(\lambda) SN(\lambda) d\lambda \right) \quad (2.8)$$

$$= m'_I - 2.5 \log \left(\frac{\int F_R(\lambda) SN(\lambda) d\lambda \int F_N(\lambda) G(\lambda) d\lambda}{\int F_N(\lambda) SN(\lambda) d\lambda \int F_R(\lambda) G(\lambda) d\lambda} \right). \quad (2.9)$$

The term inside of the log gives the difference in ratio between the new and reference counts for galaxies and supernovae. Note that the reference image defines the instrumental system and that if the new and reference images are taken with instruments with the same transmission efficiencies then $m_I = m'_I$.

Transforming the instrumental magnitude into a Johnson-Cousins magnitude requires the observation of photometric calibrators. Ideally the magnitude of the supernova is the instrumental magnitude plus the zeropoint determined from "standard supernovae" with observed magnitudes m_{0I} and tabulated magnitudes m_0 :

$$m = m_I + (m_0 - m_{0I})|_{SN}. \quad (2.10)$$

Since there are no such things as "standard supernovae," we instead measure standard stars, given as $(m_0 - m_{I0})|_S$:

$$m = m_I + (m_0 - m_{0I})|_S - 2.5 \log \left(\frac{\int F_R(\lambda) S(\lambda) d\lambda \int F_{J-C}(\lambda) SN(\lambda) d\lambda}{\int F_R(\lambda) SN(\lambda) d\lambda \int F_{J-C}(\lambda) S(\lambda) d\lambda} \right). \quad (2.11)$$

The term inside of the log describes the different way standard star and supernova instrumental magnitudes are transformed to the Johnson-Cousins system.

We finally obtain the standard supernova magnitude from our galaxy subtracted,

standard star calibrated photometry,

$$m = m'_I + (m_0 - m_{I0})|_S + C, \quad (2.12)$$

where

$$C = -2.5 \log \left(\frac{\int F_R(\lambda)S(\lambda)d\lambda}{\int F_N(\lambda)SN(\lambda)d\lambda} \frac{\int F_N(\lambda)G(\lambda)d\lambda}{\int F_R(\lambda)G(\lambda)d\lambda} \frac{\int F_{J-C}(\lambda)SN(\lambda)d\lambda}{\int F_{J-C}(\lambda)S(\lambda)d\lambda} \right). \quad (2.13)$$

The first two terms of Equation 2.12 are what we actually get from the galaxy subtraction and standard star calibration as our magnitude. C is a second order systematic correction accounting for the differences between supernovae and standard stars and supernovae and galaxies. Note that C is a function of supernova epoch and presumably on the supernova light-curve width. The spectrum used to calculate C must therefore be selected appropriately based on the supernova being corrected.

We have produced effective transmission functions by convolving the filter transmission, CCD quantum efficiency, and the atmospheric extinction from each of the sites for the telescopes we have used. The supernova spectra are those of the nearby supernovae SN 1981B, SN 1990N, and SN 1992A redshifted out to the relevant redshifts. I plot in the following pages C as a function of supernova epoch for some of the relevant filter combinations and redshifts. All epochs are in the supernova rest frame. The Kitt Peak 2m and the INT Harris filter systems are similar to the realization of the Cousins R band produced by Bessell (1990).

These are just a few of the filter combinations and supernovae for which we have data. We can make a few comments based on these plots. First, the data taken

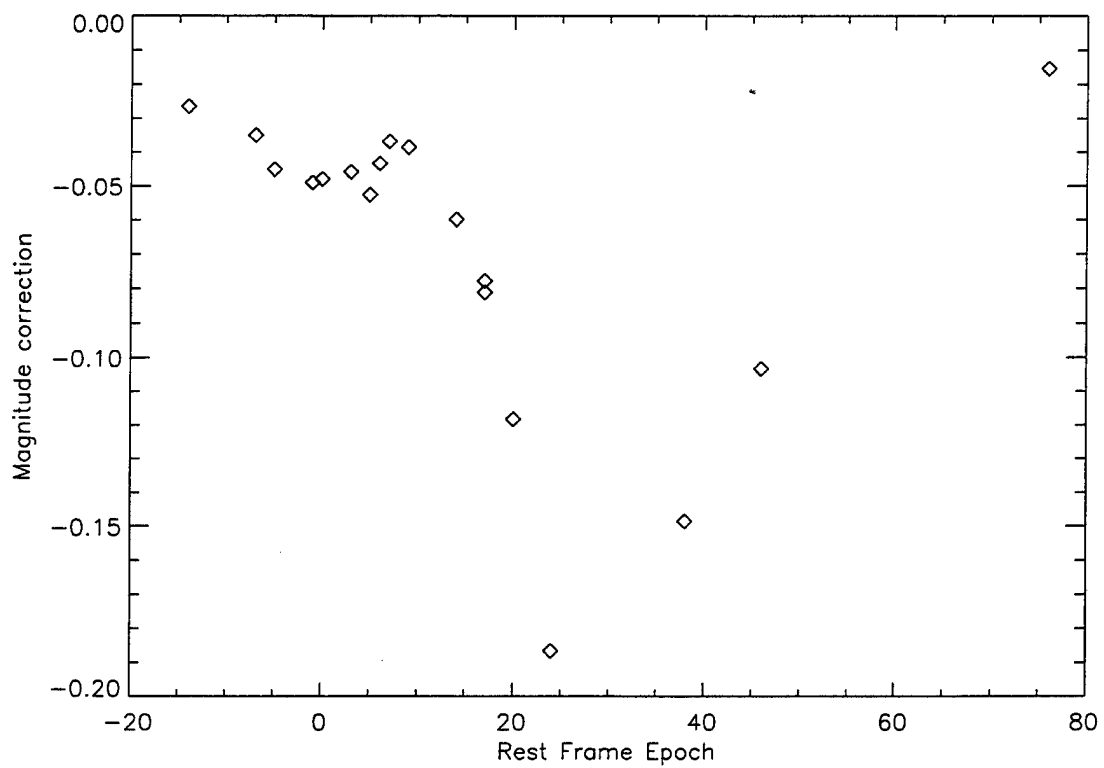


Figure 2.4: Instrumental Corrections at $z = 0.374$ for INT images taken with the Mould filter and KP2m references.

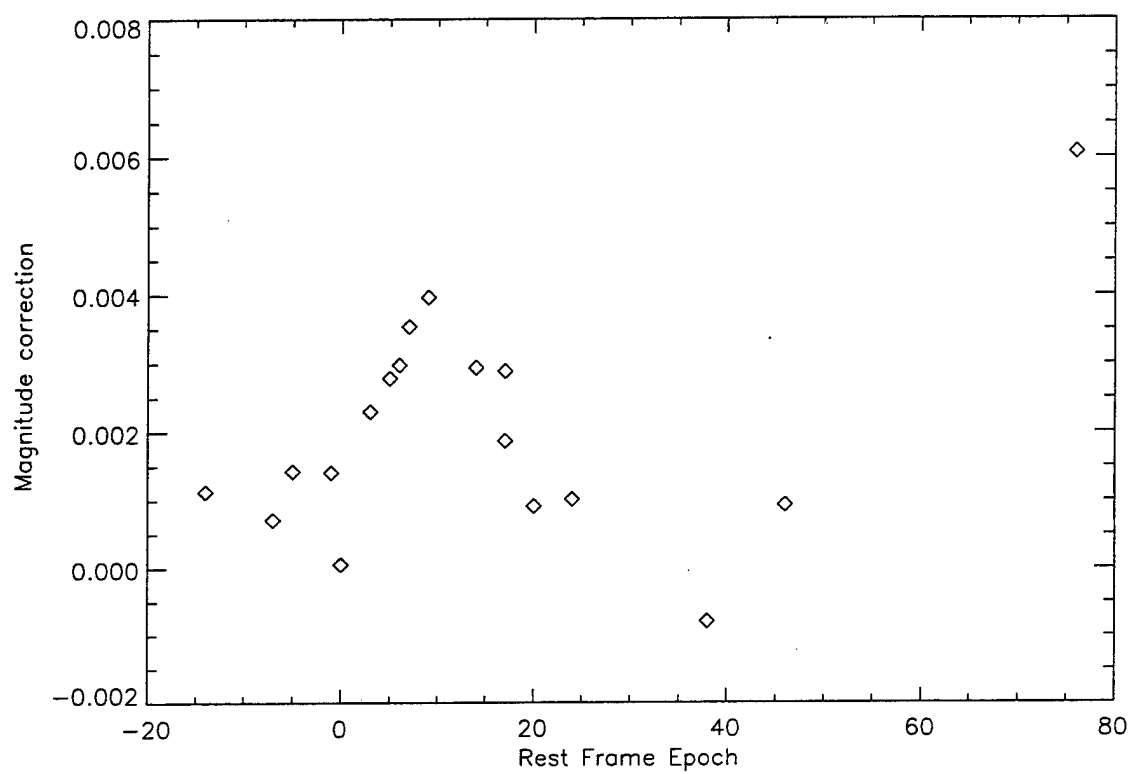


Figure 2.5: Instrumental Corrections at $z = 0.374$ for INT images taken with the Harris filter and KP2m references.

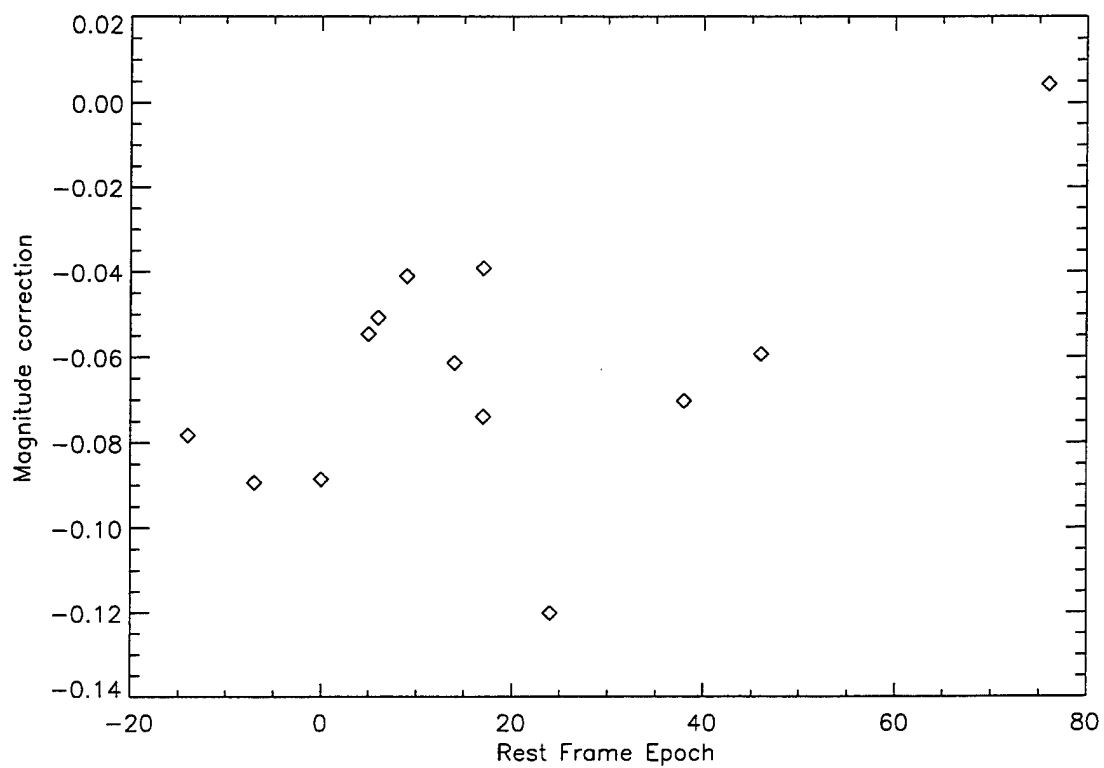


Figure 2.6: Instrumental Corrections at $z = 0.42$ for INT images taken with the Mould filter and KP2m references.

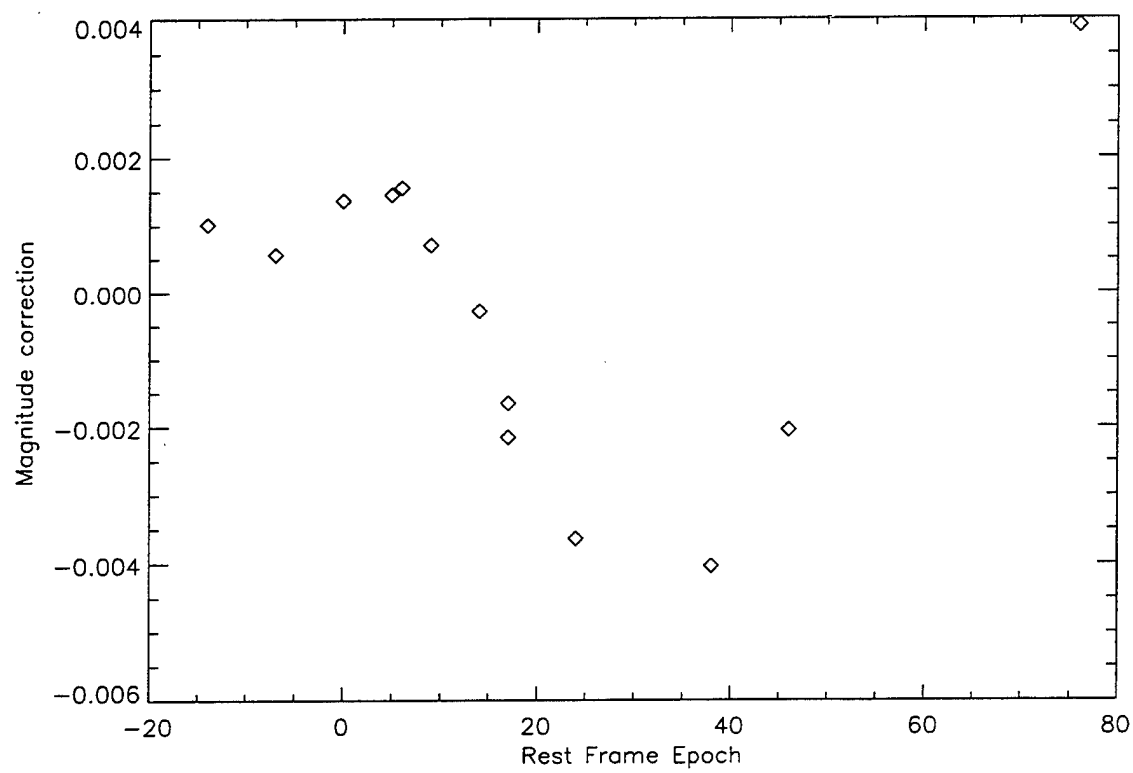


Figure 2.7: Instrumental Corrections at $z = 0.42$ for INT images taken with the H_α filter and KP2m references.

with the Mould filter require a relatively large correction (compared to data taken with the Harris filter) that will make the supernova *brighter*. Second, most of the curves show a dependence on epoch. Third, although both the KP4m and Harris are Cousins filters, they do not behave identically. Slight differences in filter, CCD, and atmospheric transmission produce differences in the total transmission that give the slightly different results.

The handling of all the uncorrelated errors is simple; their squares are added in as diagonal elements in the light curve covariance matrix, i.e., $V_{ii} = V_{ii} + \sigma_{i,total}^2$. The final covariance matrix, which includes all uncorrelated and correlated errors, is used for statistical analysis of the light curve.

Chapter 3

K Corrections

[This chapter has been published by A. Kim, A. Goobar, & S. Perlmutter under the title “A Generalized K Correction for Type Ia Supernovae: Comparing R-band Photometry Beyond $z = 0.2$ with B, V, and R-band Nearby Photometry”, in the Publications of the Astronomical Society of the Pacific, 108:190–201, 1996.]

Magnitudes of local and distant supernovae, both in the same filter band, are compared using a K correction to account for the different spectral regions incident on that filter. A generalized approach compares magnitudes in different bands for the nearby and distant supernovae, bands that are selected to give sensitivity in corresponding regions of the unredshifted and redshifted spectra. Thus, R magnitudes for supernovae at $z \approx 0.5$ are compared with B magnitudes of local supernovae. We compute these generalized K corrections over a range of redshifts and bandpass

pairs and discuss their advantages over the traditional single-band K correction. In particular, errors near maximum light can be kept below 0.05 mag out to at least $z = 0.6$, whereas the traditional K correction is less accurate and can be difficult to determine beyond $z > 0.2$.

3.1 Introduction

Given a homogeneous set of Type Ia supernovae and assuming no evolution, a perfect and complete catalog of Type Ia spectra can be used to calculate the apparent magnitudes at any redshift and for any particular date with respect to maximum light. In practice, this is not feasible due to several problems: (1) The available supernova spectra often have insufficient wavelength coverage to calculate broadband photometry and insufficient time coverage to track the quickly evolving supernova; (2) Many of the available spectra do not have the signal-to-noise ratio to calculate precise magnitudes; (3) Spectral miscalibrations can lead to large errors in magnitude determinations; (4) The filter transmission function and detector response function are not perfectly known; (5) Even within the subset of Type Ia's with remarkably similar spectra, there are minor differences that can lead to slight supernova-to-supernova variation in magnitude. More reliable magnitude calculations can be made using spectra and photometry together, photometry being less sensitive to most of the above problems than spectra. In this paper, we calculate and discuss the errors for a generalized K correction, an example of such a technique, with a preliminary analysis using

three Type Ia supernova. (One “peculiar” Type Ia supernova was also examined for comparison purposes.) These K corrections are particularly important for use with supernovae at $z > 0.2$, which are now being discovered in systematic searching (e.g., Perlmutter et al. 1994, 1995). Analysis of standard K corrections for Type Ia supernovae, useful for lower redshifts, have been performed by Hamuy et al. (1993) and Leibundgut (1990).

3.2 A Generalized K Correction

The standard K correction, K_x , is used to calculate the apparent magnitude in some “ x ” filter band of an object at redshift z according to the equation $m_x(z, t) = M_x(t) + \mu(z) + K_x(z, t)$, where μ is the distance modulus (based on luminosity distance) and M_x is the absolute x magnitude (we omit explicit time dependence in subsequent equations). The K correction relates nearby and distant magnitudes measured with the same filter:

$$K_x = 2.5 \log(1 + z) + 2.5 \log \left(\frac{\int F(\lambda) S_x(\lambda) d\lambda}{\int F(\lambda/(1 + z)) S_x(\lambda) d\lambda} \right), \quad (3.1)$$

where $F(\lambda)$ is the spectral energy distribution at the source (in this case the supernova), and $S_x(\lambda)$ is the x 'th filter transmission (Oke & Sandage 1968).

We generalize this expression to handle different filters, adding a term that ac-

counts for the differences in the zeropoints of the magnitude system:

$$\begin{aligned}
 K_{xy} &= -2.5 \log \left(\frac{\int Z(\lambda) S_x(\lambda) d\lambda}{\int Z(\lambda) S_y(\lambda) d\lambda} \right) + 2.5 \log(1+z) \\
 &\quad + 2.5 \log \left(\frac{\int F(\lambda) S_x(\lambda) d\lambda}{\int F(\lambda/(1+z)) S_y(\lambda) d\lambda} \right) \\
 &= -2.5 \log \left(\frac{\int Z(\lambda) S_x(\lambda) d\lambda}{\int Z(\lambda) S_y(\lambda) d\lambda} \right) + 2.5 \log \left(\frac{\int F(\lambda) S_x(\lambda) d\lambda}{\int F(\lambda') S_y(\lambda'(1+z)) d\lambda'} \right) \quad (3.2)
 \end{aligned}$$

where $Z(\lambda)$ is an idealized stellar spectral energy distribution at $z = 0$ for which $U = B = V = R = I = 0$ in the photometric system being used. K_{xy} is thus defined so that $m_y = M_x + \mu + K_{xy}$. If $S_x \equiv S_y$, the first term drops out and this reduces to the standard K correction of Equation 3.1.

The second line of Equation 3.2 is a change of variables, $\lambda' = \lambda/(1+z)$, that makes it easier to understand the K_{xy} correction in the case $S_y(\lambda(1+z)) = S_x(\lambda)$, a situation approximated by the dashed lines in Figure 3.1. If the “blueshifted” y ’th filter matches the x ’th filter function the second term in this equation drops out, and one is left with the term accounting for the difference in zeropoints of the filters (this difference is the “color zeropoint”). In this case, spectral dependence on the correction is eliminated. Note that this cross-filter approach has previously been used for galaxy K corrections (e.g. Gunn 1978).

3.3 K_{xy} Calculation

We calculate generalized K corrections using Equation 3.2 with Bessell’s (1990) color zeropoints and realizations of the Johnson-Cousins UBVRI filter system (Fig-

ure 3.1). The color zeropoints are expected to match real photometric color zeropoints to better than 0.01 mag (Hamuy et al. 1992 quotes ≤ 0.009 , Bessell (private communication) quotes ≤ 0.005). We use the same sample of supernova spectra as Hamuy et al. (1993), excluding those of SN 1991T from the main analysis as it was spectroscopically peculiar (Filippenko et al. 1992; Phillips et al. 1992), and including spectra of SN 1981B, a supernova that has been frequently used as a template Type Ia.

Our full sample is presented in Table 1 and contains 29 spectra from epochs $-14 < t_{max}^B < 76$ days (in the supernova rest frame) after blue maximum for SN 1981B, SN 1990N, and SN 1992A. The SN 1981B data is from Branch et al. (1983), SN 1990N data is described in Leibundgut et al. (1991), and SN 1992A is in Suntzeff et al. (1995), and Kirshner et al. (1993). The SN 1981B spectra labeled by epoch (0) is a composite of four spectra from March 6-9 (Branch et al. 1983). The SN 1992A HST spectra from epoch 5 with a spectral range of 1650-4800 Å has been augmented by the CTIO spectra from epoch 6 as described in Kirshner et al. (1993); it is labeled epoch (5). The K corrections were not calculated for cases in which the spectra did not cover at least 99% of the effective acceptance of the passband; these cases are labeled with ellipses in the tables.

Tables 2, 3, and 4 have K_{xy} corrections for $x = B, V, R$, $y = R$ and redshifts spanning from 0 to 0.7 in increments of 0.025. Epochs are given in the supernova rest-frame. Note that K_{RR} is just the standard R band K correction. Each column of data

is for a single supernova spectrum; the three tables have different number of columns because the number of spectra with sufficient wavelength coverage to calculate each correction varies. In particular, Table 4 has much fewer entries because there are only a few spectra covering the needed wavelength range to calculate K_{RR} . See Hamuy et al. (1993) for tables of K_{BB} and K_{VV} ; these K corrections have poor spectral coverage at $z > 0.1$ for K_{BB} and at $z > 0.3$ for K_{VV} because at those redshifts the rarely observed near-UV region of the spectrum is redshifted into the relevant bands.

3.4 Error Estimates and Determination of Optimal Filter Pair

We consider the contributions of the following sources of error in the K correction: numerical integration error, spectral measurement and calibration error, intrinsic supernova-to-supernova dispersion, instrumental effects, and zeropoint uncertainty. We perform all analyses for each individual redshift between 0 and 0.7 in steps of 0.025. We illustrate our analysis techniques by presenting results for the specific redshift of $z = 0.5$, although our final conclusions will be based on the full analysis for all redshifts. Note that the example of redshift $z = 0.5$ demonstrates both a good filter match case (for K_{BR}) and a poor filter match case (for K_{VR}).

The numerical integration is accurate to 0.005 mag and we are able to reproduce the standard K corrections in B and in V of Hamuy et al. (1993) to that accuracy. A

larger source of uncertainty comes from the noise and calibration error of the spectra themselves. Lacking prior spectral error information, we test each spectrum's error properties by calculating, for $z = 0$, $B - V$ colors on the subset of 24 spectra with sufficient coverage. (This test was also performed in Hamuy et al.) The differences between these $B - V$ colors and the photometrically observed colors form a Gaussian distribution with a sigma of 0.04 mag. These $B - V$ colors compare two spectral regions that have little overlap, while K corrections that compare overlapping regions are less sensitive to large scale miscalibrations and therefore should have smaller error.

The rapid but smooth evolution of supernova spectra should make K corrections a smooth function on the scale of a few days. However, the data shows scatter from measurement and calibration error in the spectra. The good temporal sampling of SN 1992A allows us to make K correction error estimates based on this scatter. We illustrate by considering the specific examples of K_{BR} and K_{VR} at $z = 0.5$, shown in Figures 3.2 and 3.3. (Unfortunately, there are insufficient data points to similarly consider K_{RR} .) We first study the subset of SN 1992A K corrections calculated from spectra measured at a single telescope, the CTIO 1.0-m. This includes all SN 1992 spectra except the ones at epochs 5, 6, 9, 17, 46, and 76. We estimate the root-mean-square scatter of the data from a smooth curve to be < 0.002 for K_{BR} and < 0.02 for K_{VR} ; we take this to be the bound on the effects of spectral measurement errors. Considering the full sample of K corrections for SN 1992A from all the telescopes, we find the range (not the root-mean-square) in scatter to be ~ 0.004 for K_{BR} and

~ 0.1 for K_{VR} ; we take these to be the bounds on systematic instrumental error.

Having studied errors involved in the K corrections of a single Type Ia supernova, we now consider the uncertainties involved in constructing a single K correction for this entire class of supernovae. We do this by examining systematic differences between the three supernovae in our sample. Again consider K corrections for $z = 0.5$ plotted in Figures 3.2 and 3.3. The scatter at a given epoch in K_{BR} and K_{VR} is dominated by intrinsic supernova-to-supernova differences. These differences are understood as being due to the observed variance in the color evolution of these particular supernovae, particularly around 20 days after maximum when the supernovae have quickly reached their reddest color. The range of scatter is ~ 0.015 mag for K_{BR} and ~ 0.2 mag for K_{VR} ; for epochs before day 17, the range narrows to < 0.002 for K_{BR} and ~ 0.1 mag for K_{VR} .

As a preliminary test of the variation in K correction for Type Ia supernovae that are not “normal,” the K corrections of the “peculiar” Type Ia SN 1991T were also calculated (Ford et al. (1993) and Phillips et al. (1992) describe this supernova). Their scatter with respect to the K corrections of normal supernovae was within the intrinsic supernova-to-supernova dispersion discussed above, even for epochs < 14 days past maximum, when the SN 1991T spectra least resembled “normal” Type Ia spectra. Despite its spectral peculiarities, SN 1991T’s light curve shapes are similar to the other supernova light curves from our sample. Systematically different K corrections are expected for supernovae with peculiar color evolution. K corrections

of other peculiar Type Ia's (e.g. SN 1991bg) will be needed to test this.

In the above discussions, no conclusions could be made on the K_{RR} error due to sparseness of data. However, error estimates can be made based on the range of the correction. Recalling Equation 3.2, we see that K corrections are the sum of an overall offset due to the different filter zeropoints plus a spectrally dependent term. Smaller spectral terms will propagate smaller errors into the K correction than larger spectral terms. In this analysis, the relative size of the spectral term is apparent in the spread over time of the K correction, since it is the only time-dependent term. Comparing the spread over time from Figure 3.4(a) with that from Figure 3.2, we see that the spectral contribution in the standard single-filter K correction, K_{RR} , is almost twice that of K_{VR} , showing that the errors in K_{RR} are much larger than those of K_{VR} . This point is demonstrated more dramatically in Figure 3.4(a,b) where K_{BR} and K_{RR} are plotted on the same scale. It is clear that the scatter in K_{BR} is much smaller than would be expected for K_{RR} .

The transformation between instrumental and standard magnitudes, i.e. the color correction, is based on the observation of standard stars. However, supernovae and stars are spectroscopically different and will generally require different color corrections. The application of the standard star color correction thus leads to supernova magnitude error. In order to examine this effect, we "observe" a series of spectrophotometric standards to determine the color correction by convolving stellar spectra from Gunn and Stryker's (1983) spectrophotometric atlas with an instrumental pass-

band. Our instrumental passband, as plotted in Figure 3.5, is the effective Kitt Peak 4-m R passband constructed from the quantum efficiency of the TK2B CCD camera, the atmospheric transmission at the Kitt Peak site, and the KP1466 Harris R filter function. Figure 3.6 plots the difference between true R magnitudes and instrumentally determined R magnitudes *after color correction* as a function of observed $V - R$, for supernovae at the same redshifts considered before ($0 \leq z \leq 0.7$). Magnitudes of supernovae bluer than $V - R = 1.0$ match to better than 0.02 mag but redder supernovae give systematically different magnitudes. These redder supernovae are generally observed at $z > 0.6$ although at epochs greater than 15 days, supernovae will have $V - R > 1.0$ at $z > 0.45$. Application of an additional correction, in addition to the standard color correction for instrumental systems, can yield the true standard magnitude to within 0.01 mag. A more detailed analysis of potential systematics will require a more complete spectral data set and a variety of instrumental transmission functions.

There is an additional error due to zeropoint uncertainty for K_{BR} and K_{VR} mag which does not effect K_{RR} . This is an advantage of the single-filter K correction, since zeropoints cancel when comparing data in the same band. As discussed earlier, the size of this error is less than 0.01 mag.

Given these contributing sources of error, we can compare the overall uncertainties for the generalized and standard K corrections. Once again, we illustrate with the case of $z = 0.5$. K_{BR} and K_{VR} have the same zeropoint uncertainty, however at this

redshift K_{BR} has smaller errors than K_{VR} from all other sources. This includes measurement error, instrumental systematics, and supernova-to-supernova systematics. Although K_{RR} has no zeropoint error, it is otherwise expected to have errors even larger than K_{VR} . We emphasize that K_{BR} has these advantages because at $z = 0.5$, $S_R(\lambda(1+z)) \approx \text{constant} \times S_B(\lambda)$, as shown in Figure 3.1, minimizing the spectral dependence on the K correction.

The case of $z = 0.5$ is important as an extreme in which it is possible to match filters. To illustrate the errors expected for other redshifts, Figure 3.7 also shows the calculated root-mean-square scatter for the group of K corrections near peak magnitude, for SN 1992A at epochs -1 and 3 days after maximum, and SN 1981B at maximum. The root-mean-square scatter is minimized at redshifts where the filters best match, and monotonically worsens as one moves away from these redshifts. Note that the error can be kept below 0.04 mag by switching from the nearby V photometry to the nearby B photometry when comparing supernovae at $z > 0.36$.

In the preceding analyses, we have calculated the K corrections using Equation 2, which is the integral of energy flux, for consistency with previous work. Actual photometric measurements are performed with detectors that are photon counters, not bolometers. Therefore the correct K correction calculation to be used with measured photometric magnitudes is the integral of photon counts:

$$K_{xy}^{\text{counts}} = -2.5 \log \left(\frac{\int \lambda Z(\lambda) S_x(\lambda) d\lambda}{\int \lambda Z(\lambda) S_y(\lambda) d\lambda} \right) + 2.5 \log(1+z)$$

$$+2.5 \log \left(\frac{\int \lambda F(\lambda) S_x(\lambda) d\lambda}{\int \lambda F(\lambda/(1+z)) S_y(\lambda) d\lambda} \right).$$

The single filter version of this equation, i.e. a photon-count standard K correction, is given in Schneider, Hoessel, & Gunn (1983). Table 5 lists K_{BR}^{counts} corresponding to the same data and redshifts of Table 2. These tables give the preferred values to use for generalized K corrections when comparing actual photometry measurements. Figure 3.8 shows the difference between the two K corrections, $K_{BR}^{\text{energy}} - K_{BR}^{\text{counts}}$, as a function of redshift. For $z < 0.6$, the difference is less than 0.04 mag over all epochs considered.

3.5 Conclusions

We have considered a generalized K correction as an alternative to the single-band K correction for relating local and high-redshift supernova magnitudes. Error sizes depend on redshift and the filter pair combination chosen and reflect the size of the term that accounts for the different spectral regions observed in distant and local supernovae. Minimizing this term by matching filters to observe the same region reduces error and can make a generalized K correction better than a single-band K correction. Matching filters also reduces the wavelength range needed to perform K corrections, making more of the available data usable for better temporal coverage and for studies in systematic differences in supernovae. Generally, error estimates and optimal filter pair determinations at any redshift can be made using a procedure

similar to the one we have outlined for $z = 0.5$. Our analyses of $0 \leq z \leq 0.7$ show that combined statistical and systematic uncertainties in K correction determinations are within 0.05 mag. Roughly, we find that for $z < 0.1$, K_{RR} should be used, for $0.1 < z < 0.35$, K_{VR} should be used, and for $0.35 < z < 0.7$, K_{BR} should be used. By extension, objects at even higher redshifts (> 0.7) will have smaller K correction error if measured in the I band, i.e. if K_{BI} is used.

These general results for the preferred observation bands at a given redshift to “match filters” will, of course, be independent of object. However, further studies based on more supernova spectra will improve the estimates of the generalized K corrections, and help characterize the detailed dependence on supernova-to-supernova variation. In particular, it will be important to analyze more subluminous, red, and/or spectroscopically peculiar supernovae, and to search for any relation between K correction and light curve shape.

SN	Epoch ^a	UT Date	Observatory/Tel	Observer(s)
1990N	-14	1990 Jun. 26.17	MMTO/MMT	Foltz
1990N	-7	1990 Jul. 02.99	CTIO/1.5-m	Phillips
1992A	-5	1992 Jan. 14.11	CTIO/1.0-m	Winge
1981B	-1(a)	1981 Mar. 6	McDonald/2.7-m	See Branch et al. (1983)
1981B	-1(b)	1981 Mar. 6	McDonald/2.7-m	See Branch et al. (1983)
1992A	-1	1992 Jan. 18.13	CTIO/1.0-m	Winge
1981B	(0) ^b	1981 Mar. 7	McDonald/2.7-m	See Branch et al. (1983)
1981B	0	1981 Mar. 7	McDonald/2.7-m	See Branch et al. (1983)
1992A	+3	1992 Jan. 22.04	CTIO/1.0-m	Winge
1992A	(+5) ^b	1992 Jan. 24	HST	SINS ^c
1992A	+6	1992 Jan. 25.04	CTIO/1.5-m	Smith/Winkler
1992A	+7	1992 Jan. 26.04	CTIO/1.0-m	Winge
1990N	+7	1990 Jul. 17	Lick/3.0-m	Shields/Filippenko
1992A	+9	1992 Jan. 28.04	CTIO/1.5-m	Hamuy/Williams
1992A	+11	1992 Jan. 30.04	CTIO/1.0-m	Winge
1990N	+14	1990 Jul. 23.98	CTIO/4.0-m	Phillips/Baldwin
1992A	+16	1992 Feb. 04.04	CTIO/1.0-m	Winge
1981B	+17	1981 Mar. 24	McDonald/2.7-m	See Branch et al. (1983)
1992A	+17	1992 Feb. 05.04	CTIO/4.0-m	Hamuy
1990N	+17	1990 Jul. 27.16	MMTO/MMT	Huchra
1981B	+20	1981 Mar. 27	McDonald/2.7-m	See Branch et al. (1983)
1981B	+24	1981 Mar. 31	McDonald/2.7-m	See Branch et al. (1983)
1992A	+24	1992 Feb. 12.03	CTIO/1.0-m	Winge
1992A	+28	1992 Feb. 16.02	CTIO/1.0-m	Winge
1981B	+29	1981 Apr. 5	McDonald/2.7-m	See Branch et al. (1983)
1992A	+37	1992 Feb. 25.01	CTIO/1.0-m	Winge
1990N	+38	1990 Aug. 16.98	CTIO/1.5-m	Phillips
1992A	+46	1992 Mar. 05.02	CTIO/1.5-m	Phillips
1981B	+49	1981 Apr. 25	McDonald/2.1-m	See Branch et al. (1983)
1981B	+58	1981 May. 4	McDonald/2.7-m	See Branch et al. (1983)
1992A	+76	1992 Apr. 04.02	CTIO/4.0-m	Hamuy/Maza

^a Epoch relative to *B* maximum light.

^b See text for discussion.

^c Supernova Intensive Study General Observer program. Spectra described in Kirshner et al. (1993)

Table 3.1: Selected Spectra of Type Ia supernovae

z	$t_0^B = -14$															
	SN 1990N	1990N	1992A	1992A	1981B (0)	3	5	6	7	9	11	14	16			
0.000	0.024	0.107			
0.025	-0.042	0.013	...	-0.146	-0.228			
0.050	-0.094	-0.043	...	-0.204	-0.285			
0.075	-0.143	-0.128	-0.087	...	-0.263	-0.344	...	-0.387			
0.100	-0.199	-0.180	-0.146	...	-0.326	-0.408	...	-0.470			
0.125	-0.256	-0.223	-0.202	...	-0.371	-0.452	...	-0.515			
0.150	-0.296	-0.248	-0.230	...	-0.396	-0.477	...	-0.544	-0.625	...	-1.142			
0.175	-0.320	-0.271	-0.356	-0.365	-0.245	-0.418	-0.407	-0.488	-0.572	-0.560	-0.640	...	-1.135			
0.200	-0.345	-0.303	-0.372	-0.379	-0.265	-0.435	-0.424	-0.503	-0.584	-0.577	-0.654	...	-1.117			
0.225	-0.376	-0.342	-0.398	-0.408	-0.306	-0.467	-0.463	-0.538	-0.616	-0.618	-0.695	...	-1.118			
0.250	-0.414	-0.388	-0.437	-0.452	-0.367	-0.512	-0.516	-0.584	-0.658	-0.665	-0.740	...	-1.116			
0.275	-0.454	-0.427	-0.474	-0.490	-0.421	-0.545	-0.550	-0.609	-0.676	-0.682	-0.748	-0.795	-1.082			
0.300	-0.488	-0.455	-0.499	-0.513	-0.453	-0.559	-0.562	-0.614	-0.675	-0.679	-0.741	-0.776	-1.039			
0.325	-0.510	-0.474	-0.514	-0.525	-0.471	-0.567	-0.574	-0.619	-0.675	-0.680	-0.738	-0.763	-0.997			
0.350	-0.532	-0.498	-0.540	-0.552	-0.502	-0.592	-0.603	-0.639	-0.686	-0.691	-0.740	-0.756	-0.955			
0.375	-0.568	-0.539	-0.583	-0.594	-0.552	-0.628	-0.636	-0.665	-0.699	-0.702	-0.738	-0.750	-0.911			
0.400	-0.615	-0.592	-0.629	-0.635	-0.606	-0.659	-0.663	-0.684	-0.707	-0.708	-0.733	-0.742	-0.867			
0.425	-0.661	-0.644	-0.662	-0.666	-0.649	-0.682	-0.685	-0.699	-0.714	-0.715	-0.732	-0.743	-0.832			
0.450	-0.696	-0.691	-0.695	-0.698	-0.691	-0.707	-0.709	-0.717	-0.726	-0.728	-0.739	-0.750	-0.803			
0.475	-0.716	-0.717	-0.716	-0.714	-0.712	-0.714	-0.711	-0.716	-0.722	-0.725	-0.729	-0.737	-0.761			
0.500	-0.715	-0.721	-0.709	-0.702	-0.701	-0.695	-0.689	-0.692	-0.694	-0.700	-0.698	-0.702	-0.704			
0.525	-0.693	-0.706	-0.684	-0.679	-0.676	-0.668	-0.663	-0.663	-0.662	-0.670	-0.659	-0.665	-0.644			
0.550	-0.654	-0.684	-0.657	-0.661	-0.659	-0.647	-0.640	-0.637	-0.632	-0.640	...	-0.631	...			
0.575	-0.607	-0.678	-0.637	-0.650	-0.652	-0.631	-0.619	-0.611	-0.600	-0.607	...	-0.592	...			
0.600	-0.562	-0.684	-0.647	...	-0.593	-0.580	...	-0.567	...	-0.549	...			
0.625	-0.522	-0.689	-0.634	...	-0.560	-0.542	...	-0.519	...	-0.498	...			
0.650	-0.480	-0.683	-0.608	...	-0.518	-0.494	...	-0.464	...	-0.441	...			
0.675	-0.427	-0.663	-0.571	...	-0.469	-0.404	...	-0.379	...			
0.700	-0.363	-0.631	-0.525	...	-0.416	-0.339	...	-0.310	...			

Table 3.2: K_{BR} for a range of redshifts. Ellipses (...) denote redshifts for which there is insufficient spectral coverage.

z	$t_0^B = 17$		17	17	17	20	24	24	24	28	29	37	38	46	58	76
	SN 1981B	1990N														
0.000	-0.558	-1.092	-1.817
0.025	-0.650	-1.157	-1.830
0.050	-0.776	-1.245	-1.847
0.075	-0.907	-1.319	-1.843
0.100	-0.985	-1.344	-1.806
0.125	-1.007	-1.165	-0.982	-0.804
0.150	-1.018	-1.161	-0.989	-0.820
0.175	-1.016	-1.149	-0.982	-0.820
0.200	-1.007	-1.126	-0.965	-0.837
0.225	-1.032	-1.123	-0.967	-0.894
0.250	-1.063	-1.120	-0.969	-0.925
0.275	-1.051	-1.085	-0.939	-0.913
0.300	-1.016	-1.039	-0.900	-0.895
0.325	-0.980	-0.995	-0.867	-0.879
0.350	-0.945	-0.951	-0.838	-0.857
0.375	-0.905	-0.906	-0.811	-0.829
0.400	-0.861	-0.864	-0.788	-0.807
0.425	-0.823	-0.831	-0.777	-0.794
0.450	-0.797	-0.804	-0.775	-0.769
0.475	-0.760	-0.763	-0.758	-0.718
0.500	-0.704	-0.707	-0.723	-0.659
0.525	-0.644	-0.652	-0.690	-0.607
0.550	-0.602	-0.660	-0.550
0.575	-0.547	-0.625	-0.484
0.600	-0.486	-0.587	-0.411
0.625	-0.422	-0.543	-0.331
0.650	-0.354	-0.493	-0.246
0.675	-0.284	-0.439	-0.155
0.700	-0.209	-0.380	-0.055

Table 3.3: Table 3.2, continued.

z	$t_0^B = -14$ SN 1990N	-7 1990N	-5 1992A	-1 1981B	-1 1981B	-1 1992A	-0 1981B	(0) 1981B	3 1992A	(5) 1992A	6 1992A	7 1992A	7 1990N	9 1992A	11 1992
0.000	0.008	0.038	-0.014
0.025	-0.058	-0.055	-0.047	-0.048	...	-0.091
0.050	-0.110	-0.111	-0.105	-0.106	...	-0.143
0.075	-0.159	-0.198	-0.156	-0.164	-0.164	...	-0.194	-0.114	...
0.100	-0.215	-0.249	-0.214	-0.227	-0.228	...	-0.251	-0.197	...
0.125	-0.272	-0.292	-0.270	-0.272	-0.272	...	-0.284	-0.243	...
0.150	-0.311	-0.317	-0.299	-0.297	-0.297	...	-0.297	-0.272	-0.27
0.175	-0.336	-0.341	-0.349	-0.331	-0.313	...	-0.319	-0.308	-0.308	-0.298	-0.300	-0.288	-0.28
0.200	-0.361	-0.373	-0.366	-0.345	-0.334	-0.323	-0.336	-0.326	-0.323	-0.310	-0.306	-0.305	-0.29
0.225	-0.392	-0.412	-0.392	-0.369	-0.371	-0.375	-0.374	-0.362	-0.369	-0.365	-0.358	-0.343	-0.333	-0.345	-0.34
0.250	-0.430	-0.458	-0.431	-0.426	-0.430	-0.418	-0.436	-0.421	-0.414	-0.417	-0.404	-0.384	-0.369	-0.393	-0.38
0.275	-0.470	-0.497	-0.468	-0.476	-0.481	-0.456	-0.490	-0.471	-0.447	-0.451	-0.430	-0.403	-0.388	-0.410	-0.39
0.300	-0.504	-0.525	-0.493	-0.504	-0.512	-0.479	-0.521	-0.499	-0.460	-0.464	-0.434	-0.402	-0.388	-0.407	-0.38
0.325	-0.526	-0.543	-0.507	-0.518	-0.529	-0.492	-0.539	-0.512	-0.468	-0.476	-0.439	-0.401	-0.388	-0.408	-0.38
0.350	-0.548	-0.567	-0.534	-0.540	-0.557	-0.518	-0.570	-0.540	-0.493	-0.504	-0.459	-0.413	-0.400	-0.419	-0.38
0.375	-0.584	-0.609	-0.577	-0.582	-0.607	-0.560	-0.621	-0.586	-0.529	-0.537	-0.485	-0.426	-0.421	-0.430	-0.38
0.400	-0.631	-0.662	-0.622	-0.629	-0.662	-0.602	-0.674	-0.636	-0.560	-0.565	-0.505	-0.434	-0.440	-0.435	-0.37
0.425	-0.677	-0.714	-0.656	-0.663	-0.705	-0.633	-0.718	-0.669	-0.583	-0.586	-0.519	-0.440	-0.454	-0.442	-0.37
0.450	-0.712	-0.760	-0.689	-0.664	-0.759	...	-0.608	-0.610	-0.537	-0.453	...	-0.456	-0.38
0.475	-0.732	-0.787	-0.709	-0.680	-0.781	...	-0.616	-0.612	-0.536	-0.448	...	-0.453	-0.37
0.500	-0.731	-0.791	-0.703	-0.668	-0.769	...	-0.596	-0.591	-0.512	-0.421	...	-0.428	-0.34
0.525	-0.709	-0.775	-0.678	-0.645	-0.745	...	-0.569	-0.564	-0.483	-0.388	...	-0.397	-0.30
0.550	-0.669	-0.754	-0.651	-0.628	-0.727	...	-0.548	-0.542	-0.457	-0.359	...	-0.368	...
0.575	-0.623	-0.747	-0.631	-0.616	-0.721	...	-0.532	-0.520	-0.431	-0.327	...	-0.334	...
0.600	-0.578	-0.754	-0.716	-0.495	-0.401	-0.294	...
0.625	-0.538	-0.759	-0.703	-0.461	-0.362	-0.247	...
0.650	-0.496	-0.753	-0.677	-0.419	-0.315	-0.192	...
0.675	-0.443	-0.732	-0.639	-0.371	-0.131	...
0.700	-0.379	-0.701	-0.594	-0.317	-0.066	...

Table 3.4: K_{VR} for a range of redshifts. Ellipses (...) denote redshifts for which there is insufficient spectral coverage.

z	$t_0^B = 14$ SN 1990N	16 1992A	17 1981B	17 1992A	17 1990N	20 1981B	24 1981B	24 1992A	28 1992A	37 1992A	38 1990N	46 1992A	49 1981B	76 1992A
0.000	0.222	-0.072	-0.532
0.025	0.131	-0.137	-0.545
0.050	0.004	-0.226	-0.562
0.075	-0.127	-0.300	-0.558	-0.442	-0.348
0.100	-0.205	-0.324	-0.521	-0.418	-0.349
0.125	-0.227	-0.311	-0.283	-0.308	-0.460	-0.376	-0.330	...	-0.272
0.150	...	-0.303	-0.237	-0.307	-0.290	-0.288	-0.400	-0.342	-0.335	...	-0.343	-0.316	...	-0.289
0.175	...	-0.296	-0.236	-0.295	-0.282	-0.258	-0.333	-0.310	-0.306	-0.330	-0.301	-0.288	-0.275	-0.288
0.200	...	-0.278	-0.227	-0.273	-0.266	-0.219	-0.257	-0.267	-0.267	-0.283	-0.251	-0.256	-0.246	-0.305
0.225	...	-0.279	-0.252	-0.270	-0.268	-0.205	-0.199	-0.233	-0.236	-0.250	-0.221	-0.248	-0.249	-0.363
0.250	...	-0.277	-0.283	-0.266	-0.270	-0.196	-0.146	-0.197	-0.200	-0.215	-0.190	-0.234	-0.247	-0.393
0.275	-0.327	-0.243	-0.270	-0.231	-0.240	-0.153	-0.068	-0.142	-0.142	-0.162	-0.132	-0.192	-0.209	-0.382
0.300	-0.308	-0.200	-0.236	-0.185	-0.201	-0.095	0.019	-0.082	-0.083	-0.105	-0.069	-0.143	...	-0.364
0.325	-0.295	-0.158	-0.200	-0.141	-0.168	-0.038	0.102	-0.023	-0.025	-0.050	-0.009	-0.097	...	-0.347
0.350	-0.288	-0.116	-0.165	-0.097	-0.139	0.018	0.181	0.037	0.034	0.007	0.053	-0.050	...	-0.325
0.375	-0.281	-0.072	-0.125	-0.052	-0.112	0.075	0.258	0.098	0.094	0.065	0.113	-0.002	...	-0.298
0.400	-0.274	-0.029	-0.080	-0.010	-0.089	0.132	0.330	0.155	0.150	0.118	0.168	0.037	...	-0.275
0.425	-0.275	0.007	-0.043	0.023	-0.078	0.174	0.388	0.205	0.196	0.161	0.207	0.062	...	-0.262
0.450	-0.282	0.036	-0.017	0.050	-0.076	0.199	0.432	0.250	0.239	0.201	0.237	0.086	...	-0.237
0.475	-0.269	0.078	0.020	0.091	-0.059	0.232	0.484	0.308	0.295	0.256	0.284	0.133	...	-0.187
0.500	-0.234	0.135	0.076	0.147	-0.024	0.285	0.552	0.376	0.360	0.323	0.347	0.190	...	-0.128
0.525	-0.197	0.195	0.137	0.202	0.010	0.335	0.616	0.442	0.421	0.384	0.403	0.239	...	-0.075
0.550	-0.163	0.252	0.039	0.374	0.670	0.451	0.285	...	-0.018
0.575	-0.124	0.307	0.074	0.417	0.727	0.506	0.339	...	0.048
0.600	-0.081	0.368	0.112	0.466	0.787	0.566	0.398	...	0.121
0.625	-0.030	0.432	0.156	...	0.850	0.638	0.462	...	0.200
0.650	0.027	0.500	0.206	...	0.918	0.720	0.526	...	0.286
0.675	0.089	0.570	0.260	0.805	0.592	...	0.377
0.700	0.158	0.645	0.319	0.895	0.662	...	0.476

Table 3.5: Table 3.4, continued.

z	$t_0^B = -14$ SN 1990N	0 1981B	(0) 1981B	7 1990N	17 1981B	20 1981B	24 1981B
0.000	0.000	0.000	0.000	0.000	0.000	0.000	0.000
0.025	-0.066	-0.084	-0.093	-0.078	-0.091	-0.065	-0.013
0.050	-0.118	...	-0.149	-0.129	-0.218	-0.153	-0.030
0.075	-0.167	...	-0.194	-0.180	-0.349	-0.227	-0.026
0.100	-0.223	...	-0.252	-0.237	-0.427	-0.252	0.011
0.125	-0.280	...	-0.308	-0.270	-0.449	-0.236	0.073
0.150	-0.319	...	-0.337	-0.283	-0.459	-0.216	0.132
0.175	-0.344	...	-0.352	-0.286	-0.458	-0.186	0.199
0.200	-0.369	...	-0.372	-0.292	-0.449	-0.146	0.275
0.225	-0.400	...	-0.412	-0.319	-0.474	-0.132	0.333
0.250	-0.438	...	-0.474	-0.356	-0.505	-0.123	0.386
0.275	-0.478	...	-0.528	-0.375	-0.492	-0.080	0.464
0.300	-0.512	...	-0.560	-0.375	-0.458	-0.023	0.551
0.325	-0.534	...	-0.578	-0.374	-0.422	0.034	0.634
0.350	-0.556	...	-0.608	-0.386	-0.387	0.090	0.713
0.375	-0.592	...	-0.659	-0.407	-0.347	0.148	0.790
0.400	-0.639	...	-0.712	-0.426	-0.302	0.204	0.862
0.425	-0.685	...	-0.756	-0.440	-0.265	0.247	0.920
0.450	-0.720	...	-0.798	...	-0.239	0.271	0.964
0.475	-0.740	...	-0.819	...	-0.202	0.305	1.016
0.500	-0.739	...	-0.807	...	-0.146	0.357	1.084
0.525	-0.717	...	-0.783	...	-0.085	0.407	1.148
0.550	-0.677	...	-0.765	0.447	1.202
0.575	-0.631	...	-0.759	0.489	1.259
0.600	-0.586	...	-0.754	0.538	1.319
0.625	-0.546	...	-0.741	1.382
0.650	-0.504	...	-0.715	1.450
0.675	-0.451	...	-0.677
0.700	-0.387	...	-0.632

Table 3.6: K_{RR} for a range of redshifts. Ellipses (...) denote redshifts for which there is insufficient spectral coverage. Note that only a few available spectra have sufficient wavelength coverage to make any K_{RR} calculations.

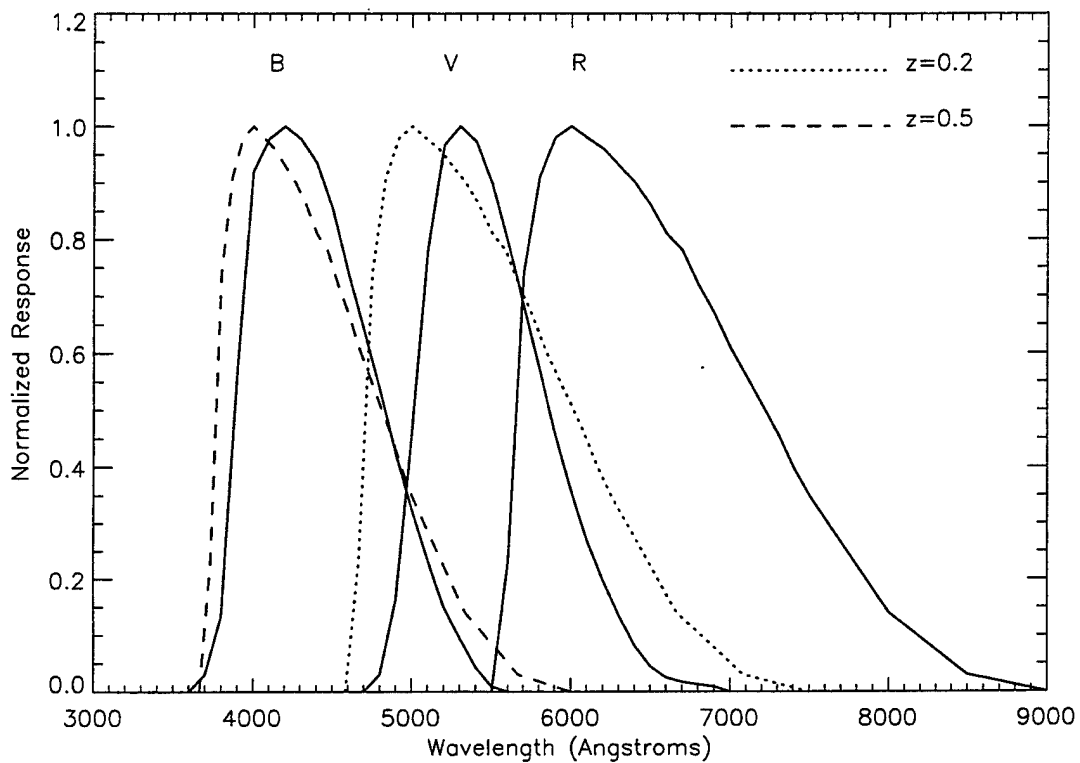


Figure 3.1: Bessell's representations of the Johnson-Cousins B , V , and R passband transmission functions, S_B , S_V , and S_R . The dotted lines represent the "blueshifted" R transmission function, $S_R(\lambda(1+z))$, at $z = 0.2$ and at $z = 0.5$. These $S_R(\lambda(1+z))$ transmission functions roughly match the $S_V(\lambda)$ and $S_B(\lambda)$ transmission functions for these values of z .

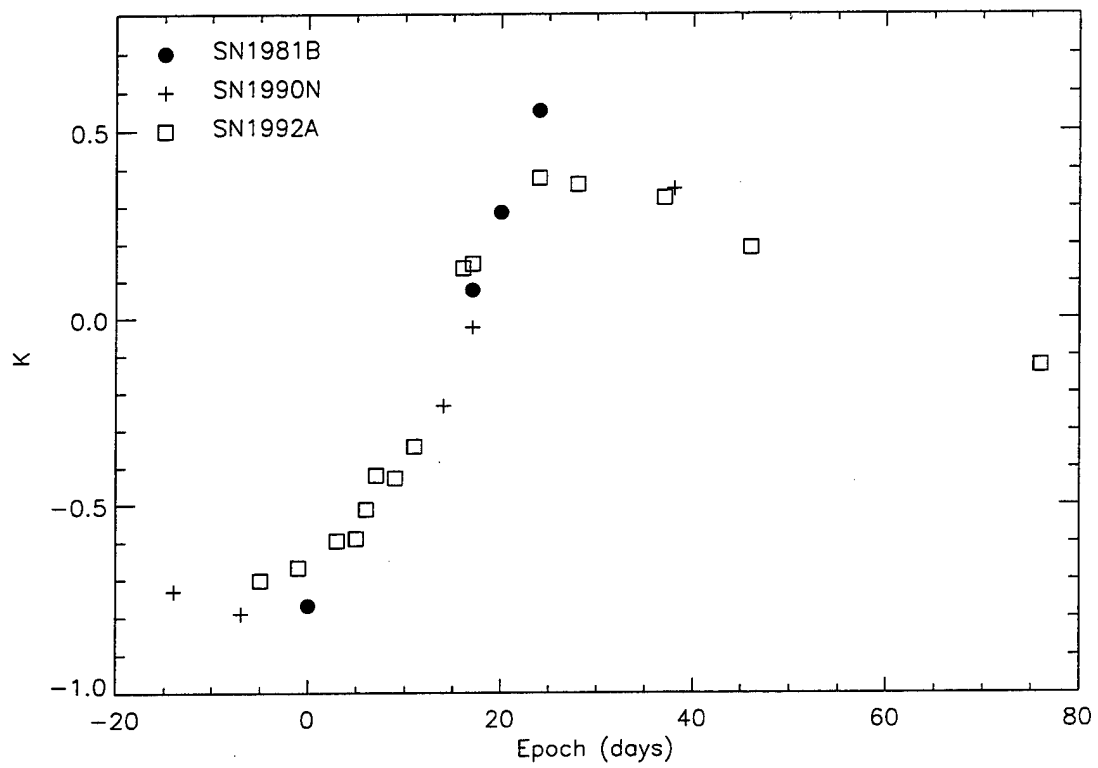


Figure 3.2: $K_{VR}(z = 0.5)$ as a function of epoch for SN 1981B, SN 1990N, and SN 1992A.

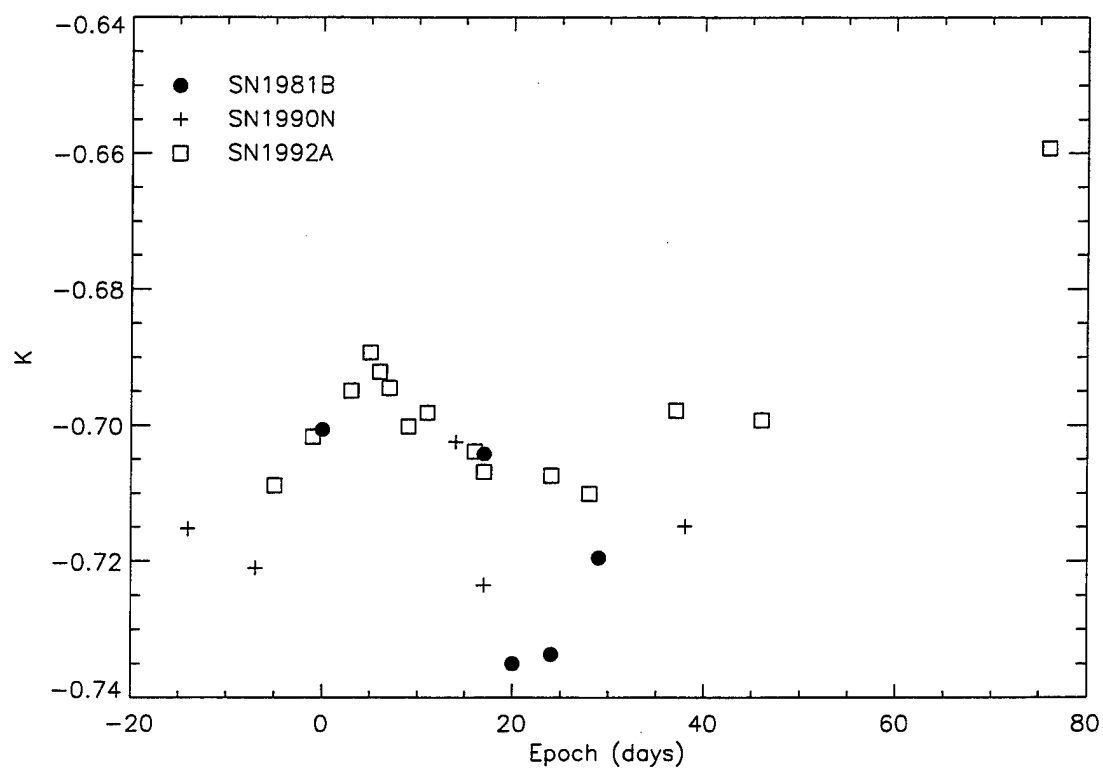


Figure 3.3: $K_{BR}(z = 0.5)$ as a function of epoch for SN 1981B, SN 1990N, and SN 1992A.

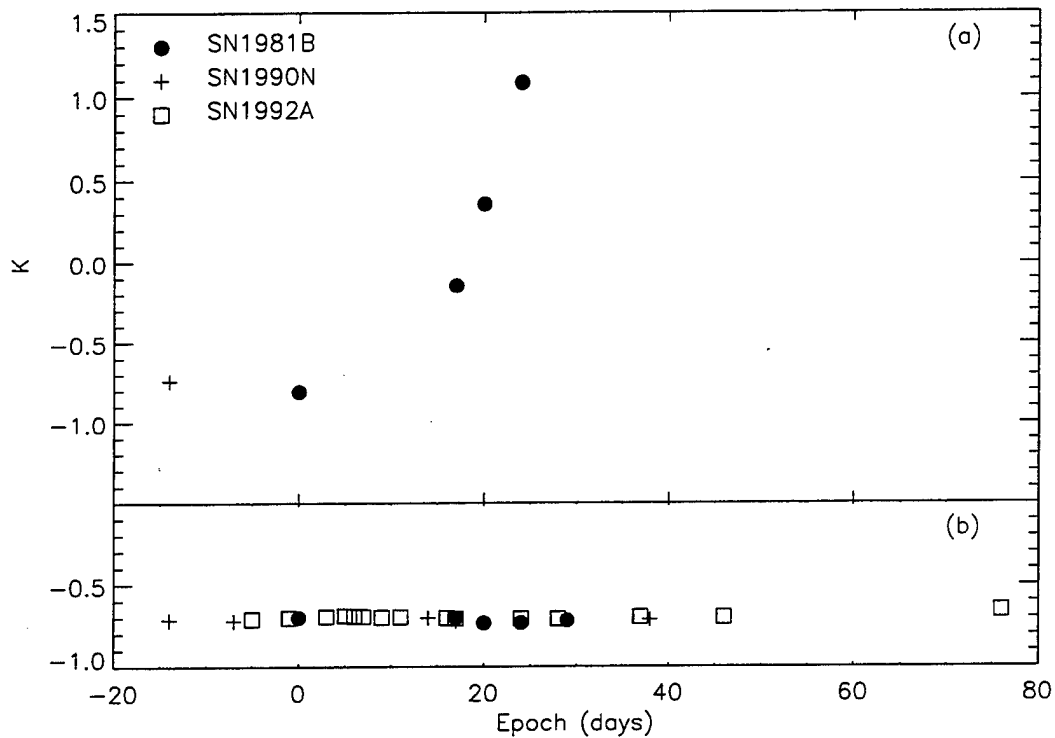


Figure 3.4: (a) $K_{RR}(z = 0.5)$ (or the R band K correction) as a function of epoch for SN 1981B and SN 1990N. The available spectra of SN 1992A do not have sufficient coverage to make such a calculation. (b) $K_{BR}(z = 0.5)$ from Figure 3 plotted on the same scale as (a) to show the much smaller range, due to the close match of the R filter at $z = 0.5$ with the B filter at rest.

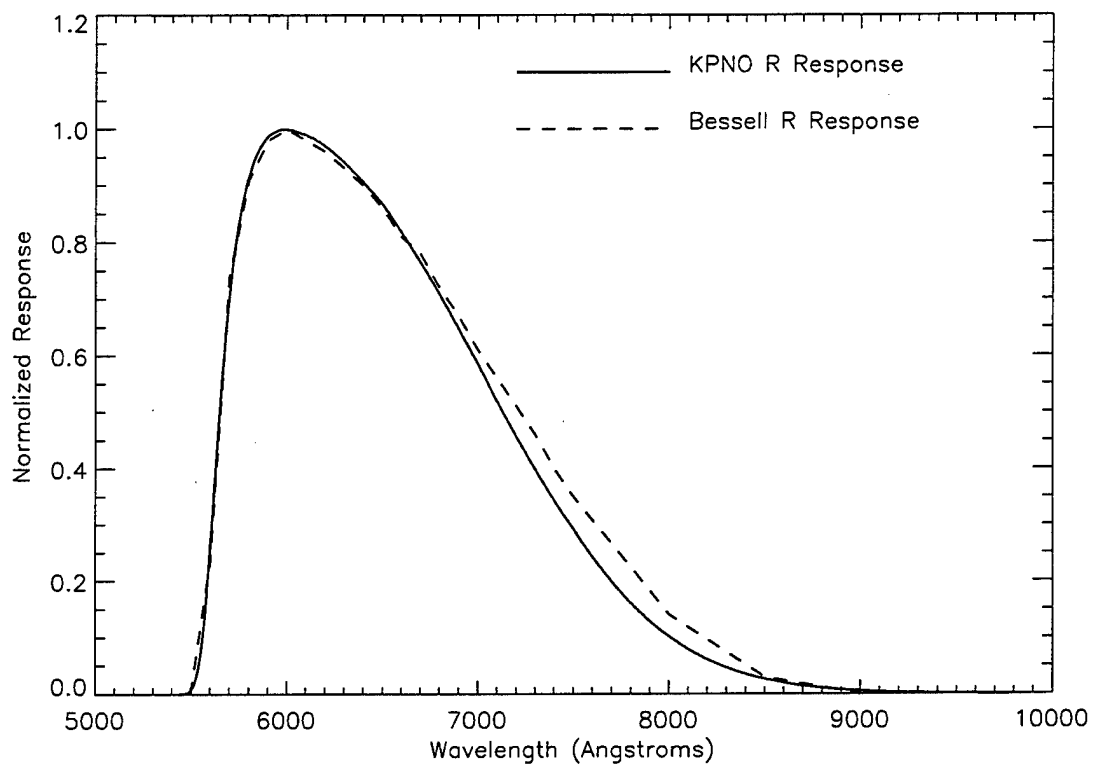


Figure 3.5: Comparison between the Bessell representation of R and our constructed response of the KPNO R as described in the text, normalized at peak transmission.

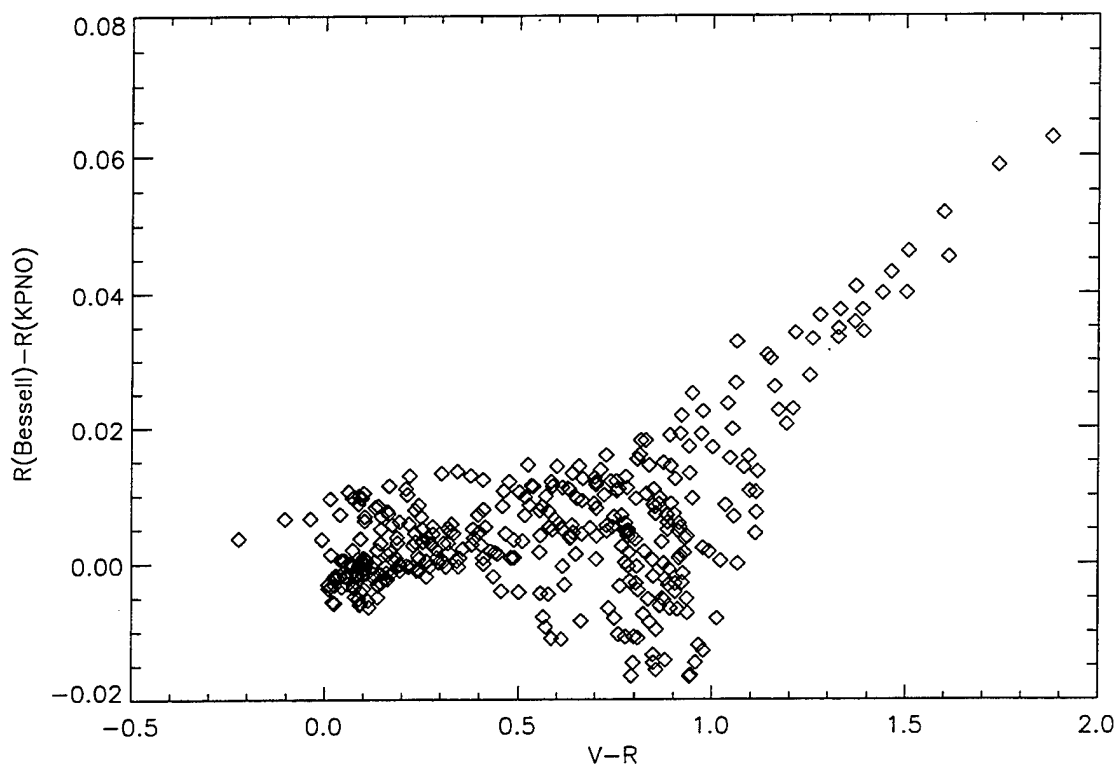


Figure 3.6: $K_{BR}^{\text{Bessell}} - K_{BR}^{\text{KPNO}}$ as a function of observed color for all redshifts.

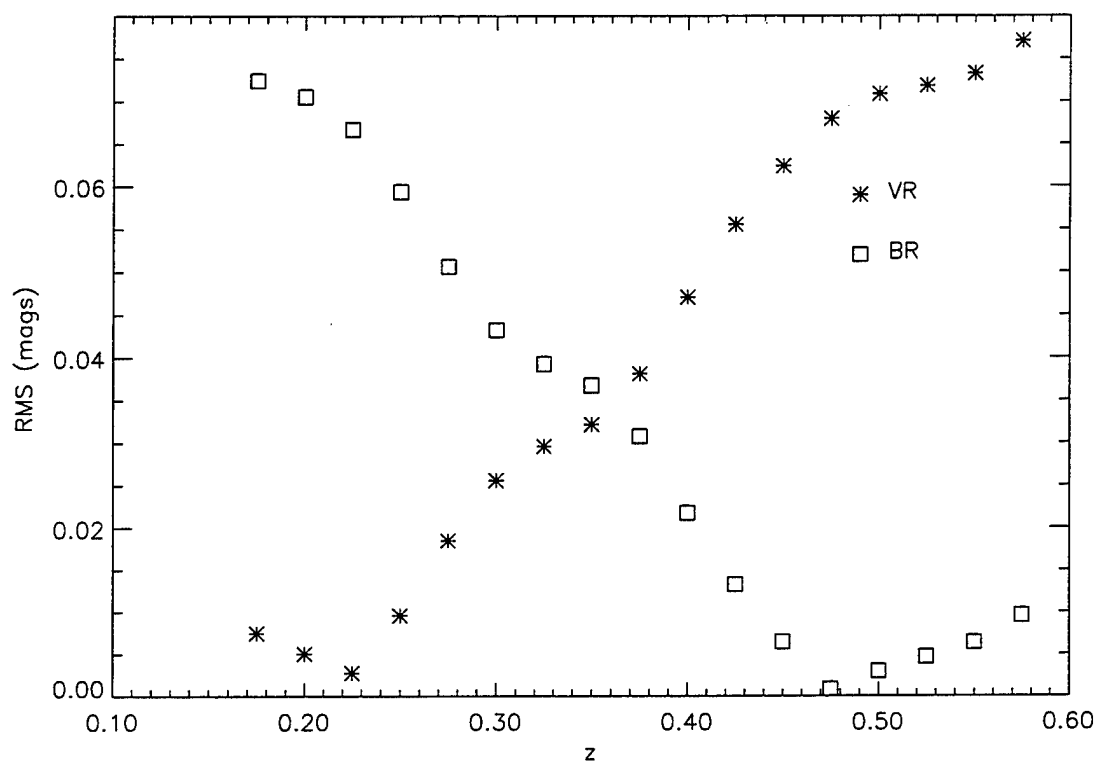


Figure 3.7: The root-mean-square scatter of K_{BR} (squares) and K_{VR} (stars) for SN 1992A at epochs -1 and 3 days after maximum, and SN 1981B at epoch 0 as a function of redshift.

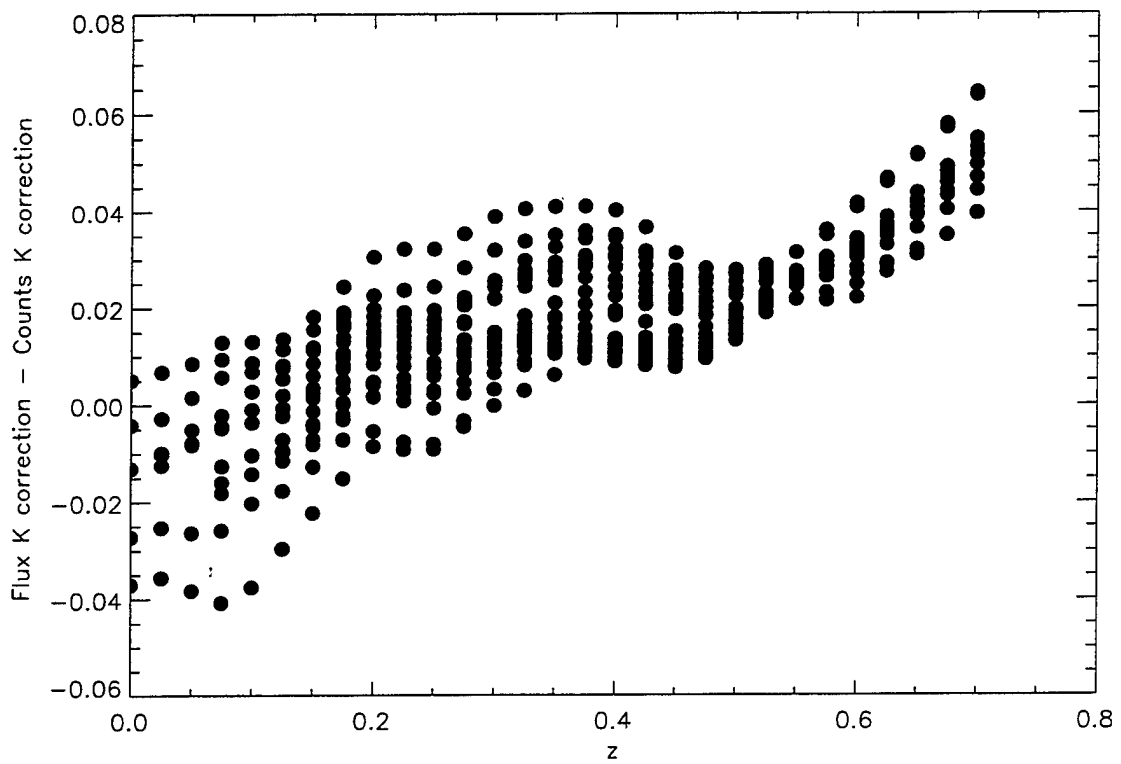


Figure 3.8: $K_{BR} - K_{BR}^{\text{counts}}$ as a function of redshift for epochs $-14 \leq t_0^B \leq 76$ days after maximum.

Chapter 4

Implications for the Hubble Constant from the First Seven Supernovae at $z \geq 0.35$

*[A condensed version of this chapter has been accepted for publication by A. Kim, S. Gabi, G. Goldhaber, D. E. Groom, I. M. Hook, M. Y. Kim, J. C. Lee, C. R. Penny-
packer, S. Perlmutter, I. A. Small, A. Goobar, R. Pain, R. S. Ellis, R. G. McMahon,
B. J. Boyle, P. S. Bunclark, D. Carter, M. J. Irwin, K. Glazebrook, H. J. M. New-
berg, A. V. Filippenko, T. Matheson, M. Dopita, & W. J. Couch under the same title
in the Astrophysical Journal Letters]*

The Supernova Cosmology Project has discovered twenty-eight supernovae at $0.35 < z < 0.65$ in an ongoing program that uses Type Ia supernovae as high-

redshift distance indicators. Here we present measurements of the ratio between the locally observed and global Hubble constants, H_0^L/H_0^G , based on the first 7 supernovae of this high-redshift data set compared with 18 supernovae at $z \leq 0.1$ from the Calán/Tololo survey. If $\Omega_M \leq 2$, then light-curve-width corrected supernova magnitudes yield $H_0^L/H_0^G < 1.20$ (95% confidence level) in a $\Lambda = 0$ universe and $H_0^L/H_0^G < 1.27$ in a flat universe. The analysis using the Type Ia supernovae as standard candles without a light-curve-width correction yields similar results. These results rule out the hypothesis that the discrepant ages of the Universe derived from globular clusters and recent measurements of the Hubble constant are attributable to a locally underdense bubble. Using the Cepheid-distance-calibrated absolute magnitudes for Type Ia supernovae of Sandage et al. (1996), we can also measure the global Hubble constant, H_0^G . Independent of Ω_M , we find that $H_0^G < 71 \text{ km s}^{-1} \text{ Mpc}^{-1}$ in a $\Lambda = 0$ universe and $H_0^G < 83 \text{ km s}^{-1} \text{ Mpc}^{-1}$ in a flat universe, correcting the distant and local supernova apparent magnitudes for light curve width. Lower results for H_0^G are obtained if the magnitudes are not width corrected.

4.1 Introduction

Some of the recent Cepheid measurements in galaxy clusters suggest a high value of the Hubble constant, $69 \leq H_0 \leq 87 \text{ km s}^{-1} \text{ Mpc}^{-1}$ (e.g., Pierce et al. 1994; Freedman et al. 1994; Tanvir et al. 1995). However, if the cosmological constant is zero, such a large Hubble constant predicts an age of the Universe that is lower than the calculated

ages of globular clusters (Bolte & Hogan 1995). To account for this discrepancy, it has been proposed that the locally (redshift $z \leq 0.05$) observed Hubble constant, H_0^L , is actually higher than the global ($z > 0.3$) Hubble constant, H_0^G (Bartlett et al. 1995). Alternatively, it may be that these Hubble constant measurements lie on the tail of their statistical and systematic error distributions. We use our first sample of seven $z > 0.35$ Type Ia supernovae to address both these possibilities, first by directly comparing our Type Ia supernova sample with one lying within the local Hubble flow to determine the ratio of H_0^L to H_0^G , and then by using our sample (the first supernovae observed in this redshift regime) together with Type Ia supernova absolute magnitude calibrations to determine the value of H_0^G .

The possibility that $H_0^L/H_0^G \neq 1$ has arisen in the context of the observation of peculiar velocity fields. The results of de Vaucouleurs (1958), Dressler et al. (1987), and Lynden-Bell et al. (1988) suggest that local measurements of the Hubble constant may differ from the mean global value. Simulations of Turner, Cen, & Ostriker (1992) have shown that measured Hubble constants depend on the observer location and the depth of observations. Previous work by Lauer & Postman (1992) has constrained deviations from uniform Hubble flow to be $\Delta H_0/H_0 < 0.07$ at $0.01 \leq z \leq 0.05$ using brightest cluster galaxies as a distance indicator. However, the same sample of galaxies shows evidence for a peculiar motion of 689 km s^{-1} with respect to the cosmic background radiation (Lauer & Postman 1994), although Riess, Press, & Kirshner (1995b) argue that Type Ia supernovae at similar redshifts do not support

this conclusion. We thus must still examine the possibility of a large scale ($z \geq 0.05$) peculiar velocity flow affecting all the local H_0 measurements.

The Supernova Cosmology Project has discovered twenty-eight supernovae in the redshift range $0.35 < z < 0.65$ in a systematic search (Perlmutter et al. 1994; 1995). This new sample of supernovae is a potentially valuable tool for cosmology: the peak magnitudes of these high-redshift candles, when compared with the peak magnitudes of local supernovae, can yield measurements of the cosmological parameters Ω_M and Λ (Goobar & Perlmutter 1995; Perlmutter et al. 1996b). This calculation implicitly assumes that the local supernova calibrators lie within the global cosmological flow; i.e., that we do not live in a local bubble where peculiar velocities appreciably bias the observed value of the Hubble constant. In this paper we take an alternative approach, leaving Ω_M and Λ as free parameters and using our high redshift Type Ia supernovae to measure (in §4.3) the ratio between the locally observed Hubble constant and the global Hubble constant, H_0^L/H_0^G .

We also use our Type Ia supernovae to obtain a measurement of the Hubble constant (§4.4). This can be compared to the other supernova-based measurements which range from $57 \text{ km s}^{-1}\text{Mpc}^{-1}$ (Sandage et al. 1996) to $\sim 66 \text{ km s}^{-1}\text{Mpc}^{-1}$ (Hamuy et al. 1995; Riess, Press, & Kirshner 1996), and to the above mentioned Cepheid methods that connect distances in a sequence from a single galaxy, to the core of its cluster, and then to the Coma cluster.

4.2 The Distant Type Ia supernova Sample

We have developed and implemented a systematic search for supernovae at redshifts $\gtrsim 0.3$. The first seven supernovae from this search were discovered between 1992 and 1994, on the rising side of their light curves. For these supernovae we obtained follow-up photometry and spectroscopy of the supernova and its host galaxy. A detailed description of our search methodology, the telescopes used, the data compiled for each event, and light curve analysis, are given in Perlmutter et al. (1996a,b).

Table 4.1 summarizes the properties of our supernovae that are relevant to this paper: the redshift as measured from the host galaxy spectrum, the best fit K-corrected B peak magnitude after our galaxy extinction correction $m_B = m_R - K_{BR} - A_R$, the value of Δm_{15} (Phillips 1993), and m_B after correction to the Leibundgut template $m_B^{\{1.1\}}$ using the relation of Hamuy et al. (1996) as discussed in §4.3. For a detailed discussion of the determination of these numbers and of the evidence for the Type Ia classification, see Perlmutter et al. (1996b). For this paper, we take these seven supernovae to be Type Ia with no evolutionary effects.

4.3 The determination of H_0^L/H_0^G

In order to use Type Ia supernovae as a cosmological candle, we first must calibrate their luminosities. If the absolute distance to a supernova is known, such as from Cepheids in the same galaxy, we can obtain the absolute magnitude M from the

apparent magnitude m . More commonly, we can only measure the redshift and an apparent magnitude. From these quantities we can obtain the intercept \mathcal{M} of the magnitude axis of the Hubble relationship, $m = 5 \log cz + \mathcal{M}$. (Following the notation of Perlmutter et al. 1996b, the script variable indicates a quantity that can be measured without knowing H_0 or the absolute distance.) These two independent observables are related at low redshifts by the relation

$$\mathcal{M} = M - 5 \log H_0 + 25, \quad (4.1)$$

where H_0 is in units of $\text{km s}^{-1}\text{Mpc}^{-1}$. We call \mathcal{M} the ‘‘Hubble intercept’’ magnitude or the ‘‘magnitude zero point’’ and we use it instead of M when studying relative values of the Hubble constant.

Progress has been made in determining both M and \mathcal{M} using nearby supernovae. The Calán/Tololo Supernova Search has discovered and measured a large sample of Type Ia supernovae within the local Hubble flow, from which a Hubble diagram with narrow magnitude dispersion can be produced and the Hubble intercept \mathcal{M} fitted. The sample includes 18 supernovae discovered no later than 5 days past maximum brightness with redshifts in the range from $3.6 < \log(cz) < 4.5$. (Of these, half are objects with $cz > 15000 \text{ km s}^{-1}$, beyond the distance of the Lauer & Postman (1994) galaxy cluster sample. However, they have magnitudes consistent with the Type Ia supernovae at lower redshift.) Using these 18 supernovae, Hamuy et al. (1996) find

$$\mathcal{M}_B = -3.17 \pm 0.03 \quad (4.2)$$

with rms dispersion $\sigma = 0.26$ mag.

Recent advances have led to a more detailed understanding of Type Ia supernovae: there is now compelling evidence that Type Ia supernovae represent a family rather than a unique set of objects. A correlation between peak magnitude and light-curve shape has been found: Phillips (1993) and Hamuy et al. (1995) parameterize the light curve with the B -band magnitude difference between peak and 15 days after peak (Δm_{15}) while Riess, Press, & Kirshner (1995a; 1996) characterize the light-curve shape by the amount (Δ) of a correction template needed to be added to a Leibundgut et al. (1991) template to get a best χ^2 fit. These parameterizations within the Type Ia class, as well as those involving spectral features (Fisher et al. 1995; Nugent et al. 1995), may make it possible to use the Type Ia supernovae as a “calibrated” candle with B magnitude dispersions of < 0.2 mag.

The Hamuy et al. (1996) sample gives a linear relation between Δm_{15} and the magnitude of the supernova, which can be expressed in terms of the Hubble intercept:

$$\mathcal{M}_{B,corr} = (0.86 \pm 0.21)(\Delta m_{15} - 1.1) - (3.32 \pm 0.05). \quad (4.3)$$

This relation is used to “correct” observed supernova magnitudes to a $\Delta m_{15} = 1.1$ standard template magnitude, $\mathcal{M}_B^{\{1.1\}}$. Applying this correction reduces the rms dispersion to $\sigma = 0.17$ mag for the observed range of Δm_{15} , between 0.8 and 1.75 mag.

Not all Type Ia supernova samples show a strong correlation between light-curve shape and peak magnitude. Sandage et al. (1996) cite the apparent lack of such a relation in the Cepheid calibrated Type Ia supernovae to argue for the use of uncor-

rected “Branch-normal” Type Ia supernovae – that is supernovae with high quality data that pass a simple $B - V$ color selection or have no spectroscopic peculiarities. This subset of Type Ia supernovae also has a low dispersion in B magnitude of ~ 0.3 mag, as shown in Vaughan et al. (1995). For this paper we therefore calculate H_0^L/H_0^G using both light-curve-shape corrected and uncorrected magnitudes.

We relate the locally derived values of the Hubble intercept and the high-redshift observed magnitudes using the standard Friedmann-Lemaître cosmology in order to measure H_0^L/H_0^G . The expected peak magnitude of a Type Ia supernova at redshift z is a function of the mass density of the universe Ω_M and the normalized cosmological constant $\Omega_\Lambda \equiv \Lambda/(3H_0^2)$:

$$m_R(z) = M_B + 5 \log(\mathcal{D}_L(z; \Omega_M, \Omega_\Lambda)) + K_{BR} + 25 - 5 \log H_0^G \quad (4.4)$$

$$= \mathcal{M}_B + 5 \log(\mathcal{D}_L(z; \Omega_M, \Omega_\Lambda)) + K_{BR} + 5 \log(H_0^L/H_0^G) \quad (4.5)$$

(e.g., Peebles 1993; Goobar & Perlmutter 1995), where K_{BR} is the K correction relating B magnitudes of nearby supernovae with R magnitudes of distant objects (Kim, Goobar, & Perlmutter 1996) and \mathcal{M}_B is measured in the local Hubble flow. Here we use \mathcal{D}_L , the “Hubble-constant-free” part of the luminosity distance, d_L :

$$\mathcal{D}_L(z; \Omega_M, \Omega_\Lambda) \equiv d_L H_0 \quad (4.6)$$

$$= \frac{c(1+z)}{\sqrt{|\kappa|}} \times \mathcal{S} \left(\sqrt{|\kappa|} \int_0^z \left[(1+z')^2 (1 + \Omega_M z') - z'(2+z')\Omega_\Lambda \right]^{-\frac{1}{2}} dz' \right) \quad (4.7)$$

where for $\Omega_M + \Omega_\Lambda > 1$, $\mathcal{S}(x)$ is defined as $\sin(x)$ and $\kappa = 1 - \Omega_M - \Omega_\Lambda$; for

$\Omega_M + \Omega_\Lambda < 1$, $\mathcal{S}(x) = \sinh(x)$ and κ as above; and for $\Omega_M + \Omega_\Lambda = 1$, $\mathcal{S}(x) = x$ and $\kappa = 1$, where c is the speed of light in units of km s^{-1} . We use \mathcal{M}_B from Equation 4.2 for uncorrected magnitudes, and from Equation 4.3 for light-curve-shape corrected magnitudes. For the high-redshift corrected supernova magnitudes, m_R , we use only the five supernovae whose light-curve widths lie within the range ($0.8 < \Delta m_{15} < 1.75$ mag) of the local supernovae from which the correlation was obtained: SN1994G, SN1994H, SN1994al, SN1994am, and SN1994an. The full sample of 7 high-redshift supernovae is used when no correction is applied.

Figure 4.1(a) shows the best fit values of H_0^L/H_0^G and the associated confidence interval curves for a range of Ω_M in a $\Lambda = 0$ universe, based on the light-curve-width corrected supernova magnitudes. Figure 4.1(b) is the same plot as Figure 4.1(a) but for the case of a flat universe ($\Omega_M + \Omega_\Lambda = 1$). Note that the best fit curve is more steeply sloped than for the $\Lambda = 0$ case, increasing the variation in H_0^L/H_0^G in this Ω_M range. (The same plots for the seven uncorrected magnitudes are almost identical on this scale.) Also plotted for reference are the ratios of representative high and low Hubble constant values.

Table 4.2 has the single-tailed 95% confidence limits (C.L.) for H_0^L/H_0^G in $\Lambda = 0$ and flat universes using corrected and uncorrected supernova magnitudes. The lower bounds are calculated at $\Omega_M = 0$ where H_0^L/H_0^G is a minimum. The value of H_0^L/H_0^G increases monotonically with respect to Ω_M , so to obtain an upper limit we choose an upper bound of $\Omega_M \leq 2$. Note that the tabulated numbers are one-tailed 95% C.L.

limits, unlike the two-tailed confidence intervals given in Figure 4.1.

As a cross check, we calculate our results for “Branch-normal” Type Ia supernovae with uncorrected magnitudes. Only SN1994G and SN1994an are confirmed “Branch-normal” based on their color or spectrum. The results obtained when using only these two are statistically consistent with those of the full sample. In a $\Lambda = 0$ universe, we obtain the limits $H_0^L/H_0^G > 0.79$ and $H_0^L/H_0^G < 1.27$, while for a flat universe we obtain $H_0^L/H_0^G > 0.68$ and $H_0^L/H_0^G < 1.35$.

Generally, we can calculate H_0^L/H_0^G for any $\Omega_M - \Omega_\Lambda$ pair using Equation 4.5; we have performed this calculation for a grid of points in the plane from $0 \leq \Omega_M \leq 2$ and $-2 \leq \Omega_\Lambda \leq 2$ using the five corrected supernova magnitudes. Figure 4.2 shows curves of constant H_0^L/H_0^G and associated uncertainties on the $\Omega_M - \Omega_\Lambda$ plane as determined from these calculations. Given in parentheses on the same plot are the H_0^L/H_0^G values for the same contours based on calculations from all seven uncorrected supernova magnitudes. (The corrected and uncorrected contours do not have the exact same shape in the $\Omega_M - \Omega_\Lambda$ plane due to their redshift dependence. However, their actual deviations are small within the scale of our plot and in comparison with our error bars. We thus present the results from both scenarios in a single plot.) Within the $\Omega_M - \Omega_\Lambda$ region plotted, $H_0^L/H_0^G = 70/50 = 1.4$ is excluded to $\gg 99\%$ confidence. This limit can still be lower if independent lower limits of the age of the Universe and Ω_Λ are included.

In Perlmutter et al. (1996b), we discuss the potential errors due to Malmquist

bias and host galaxy extinction. The bounds on those errors are small enough not to affect our results.

4.4 The Hubble Constant

The measurement of the global Hubble constant H_0^G , as opposed to the ratio of Hubble constants H_0^L/H_0^G , requires knowledge of the absolute magnitude M . The high resolution of the Hubble Space Telescope has made possible the discovery of Cepheids and measurement of their light curves in galaxies that have hosted well-observed Type Ia supernovae (Sandage et al. 1996; Saha et al. 1994, 1995). To date, six galaxy distances have been calculated to determine the peak absolute magnitudes of seven supernovae. The weighted mean of these supernova magnitudes is given in Sandage et al. (1996) as

$$M_B = -19.47 \pm 0.07 \text{ mag} \quad (4.8)$$

with a dispersion $\sigma = 0.16$ mag.

Six of the seven supernovae have a Δm_{15} measurement (Sandage et al. 1996), from which we calculate the weighted mean of the peak absolute magnitude of Type Ia supernovae corrected to $\Delta m_{15} = 1.1$ mag. Using the Δm_{15} vs. magnitude relation of Equation 4.3, we find

$$M_B^{\{1.1\}} = -19.45 \pm 0.07 \text{ mag} \quad (4.9)$$

with $\sigma = 0.14$ mag.

There is some debate on whether these supernovae have been properly extinction-corrected and weighted. For example, Riess, Press, & Kirshner (1996) use the correction template method mentioned above to conclude that SN1972E is significantly extinguished by its host galaxy. It has also been noted that the supernovae measured with photographic plates give magnitudes that are systematically brighter than ones measured photoelectrically. Therefore, although we use all seven (six for the Δm_{15} corrected) supernovae for our main results, we also include for comparison the Riess, Press, & Kirshner (1996) analysis of the three supernovae with photoelectric data that yields

$$M_{B,\Delta=0} = -19.36 \pm 0.1 \text{ mag} \quad (4.10)$$

for a $\Delta = 0$ Leibundgut template supernova.

Inserting the absolute magnitudes of Equations 4.8 and 4.9 into Equation 4.4, we obtain useful upper bounds of the “global” Hubble constant H_0^G , which are listed in Table 4.2. The bounds are calculated at $\Omega_M = 0$ for $\Lambda = 0$ universes and flat universes because H_0^G decreases with increasing Ω_M . If we take $\Omega_M \geq 0.2$ we obtain even tighter limits, also given in Table 4.2. Figure 4.2 shows H_0^G in the most general case, for different values of Ω_M and Ω_Λ . Note that a value of H_0 as high as $80 \text{ km s}^{-1}\text{Mpc}^{-1}$ is only found for large values of Ω_Λ and low Ω_M . As a cross check, we again calculate our results for uncorrected “Branch-normal” supernovae. We then find $H_0^G < 70 \text{ km s}^{-1}\text{Mpc}^{-1}$ in a $\Lambda = 0$ universe and $H_0^G < 82 \text{ km s}^{-1}\text{Mpc}^{-1}$ in a flat universe.

4.5 Conclusions

The measurement of cosmological distances using high-redshift supernovae with locally-calibrated standard candles sets a limit on the differences between the local and global Hubble constants. From our analysis, it is clear that these data are inconsistent with scenarios that use a local bubble with high H_0^L that differs greatly from H_0^G . We also obtain an upper limit for the Hubble constant that is consistent with many of the other current measurements. However, tighter limits that disagree with some measurements may be obtained with independent constraints on Ω_Λ .

The Type Ia supernova absolute magnitude calibrations are still subject to debate and may have systematic errors larger than the statistical ones given above, so it is important to ask how robust our results are. An uncertainty in the absolute calibration δm in magnitudes propagates into $\delta H_0/H_0 \approx \delta m$. A 0.09 mag difference in the magnitude calibrations, such as the one between the Δm_{15} -corrected absolute magnitudes for six supernovae (Equation 4.9) and that of Riess, Press, & Kirshner (1996) with their extinction corrections for three of the supernovae (Equation 4.10), will produce a 10% change in either H_0^G or H_0^L/H_0^G .

There is little difference between magnitude corrected and uncorrected results for the ratio H_0^L/H_0^G , but there is a systematic difference for H_0^G itself, as seen in Table 4.2. This is because both the light-curve-width distribution and the width-magnitude relation of our high-redshift sample are similar to the distribution and relation of the Hamuy et al. (1996) sample but not to those of the Sandage et

al. (1996) sample. Although these differences may be due to selection effects, the small number statistics of the Cepheid-calibrated supernova sample can also produce fluctuations that account for the differences.

In Perlmutter et al. (1996b) we calculated Ω_M and Ω_Λ setting H_0^L equal to H_0^G , whereas in this paper we have discussed the measurement of H_0^L/H_0^G while leaving Ω_M and Ω_Λ as free parameters. Ideally one would like to measure both sets of quantities simultaneously. (This problem has been discussed in Wu, Qin, & Fang 1996.) Filling in a Hubble diagram with measurements of spatially well-distributed supernovae should make it possible to decouple local and global streaming motions by showing redshift dependent deviations from the standard model, and allow one to measure Ω_M and Ω_Λ independently of local peculiar flows. Using supernovae from redshift regimes with no evidence of flows, we can simultaneously fit H_0^G , Ω_M , and Ω_Λ using Equation 4.4, producing an independent measurement of the Hubble constant. Our current data set, which spans from $0.35 < z < 0.5$, shows no sign of peculiar flows but needs a larger statistical sample and more complete spatial coverage to confirm this result.

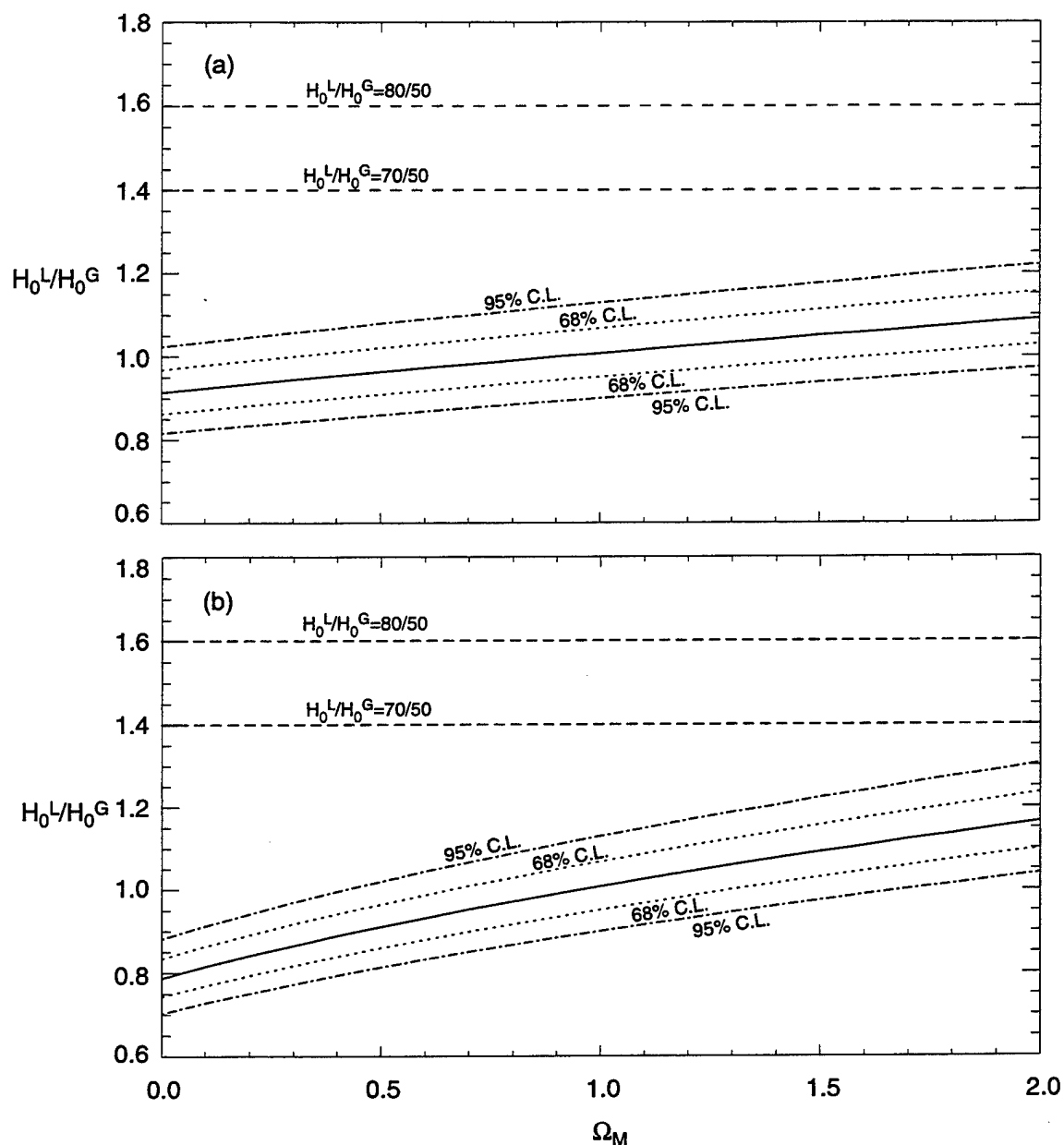


Figure 4.1: The best fit H_0^L/H_0^G with 68% (short dashes) and 95% (dot-dashes) error range for each value of Ω_M in an (a) $\Lambda = 0$ universe and (b) flat universe, using the five light-curve corrected supernova magnitudes. (These are the results from a single parameter fit; the uncertainties are calculated for each value of Ω_M .)

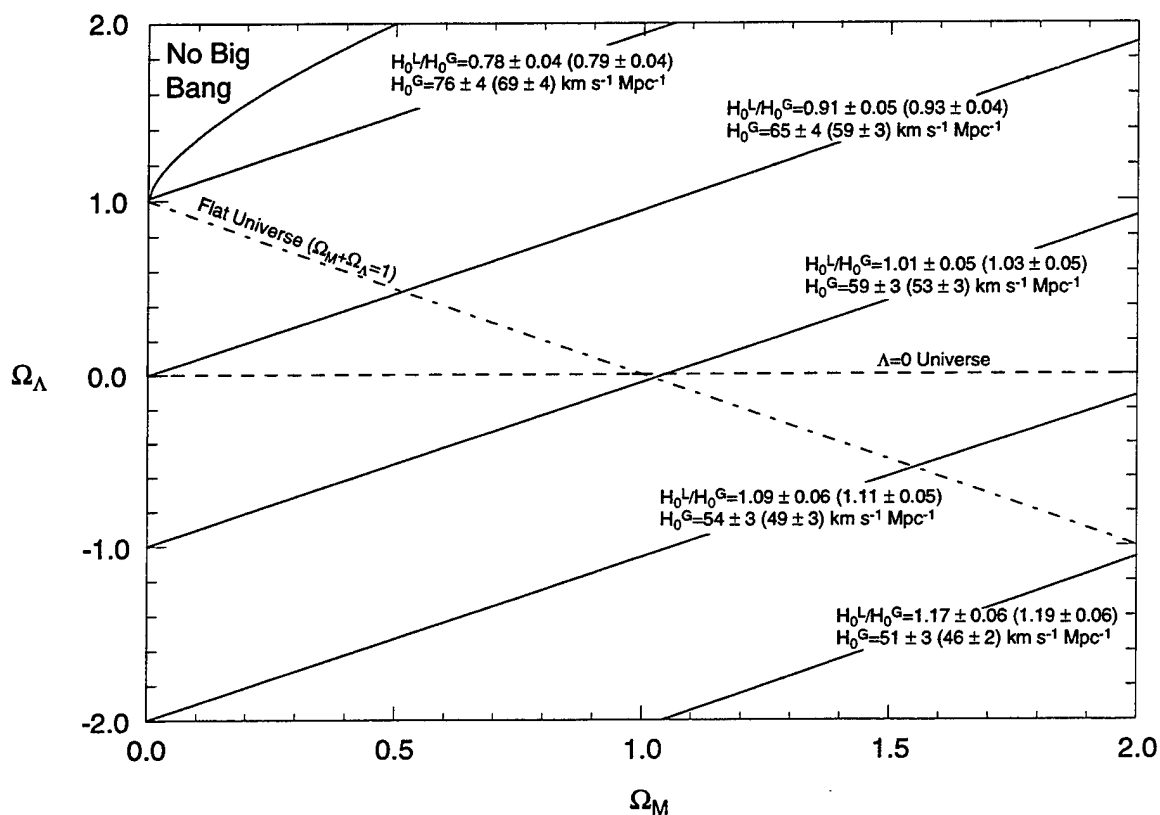


Figure 4.2: The solid lines show contours of constant H_0^L/H_0^G and H_0^G when Ω_M and Ω_Λ are fixed. They are labeled with their value and associated uncertainties based on the five corrected supernova magnitudes. The values of H_0^L/H_0^G and H_0^G derived from the seven uncorrected supernova magnitudes are given in parentheses for the approximately corresponding contour.

	SN1992bi	SN1994H	SN1994al	SN1994F	SN1994am	SN1994G	SN1994an
z	0.458	0.374	0.420	0.354	0.372	0.425	0.378
m_B	22.70 (9)	21.91 (4)	22.81 (12)	22.45 (30)	22.25 (6)	22.27 (6)	22.62 (7)
Δm_{15}	0.50 (40)	0.87(9)	1.18(20)	2.00 (61)	1.44 (12)	1.05 (3)	1.64 (29)
$m_B^{\{1.1\}}$... ^a	22.11 (10)	22.74 (21)	... ¹	21.96 (13)	22.32 (7)	22.16 (28)

^a SN1992bi and SN1994F have best fit Δm_{15} outside the range found for the nearby Type Ia

supernovae; hence, to avoid extrapolation, $m_B^{\{1.1\}}$ corrected magnitudes are not reported or used.

Table 4.1: Supernova Data and Photometry Error Budget

		H_0^L/H_0^G		H_0^G Upper limit (km s ⁻¹ Mpc ⁻¹)	
		Lower Limit	Upper Limit	$\Omega_M \geq 0$	$\Omega_M \geq 0.2$
$\Lambda = 0$	Corrected	> 0.83	< 1.20	< 71	< 70
	Uncorrected	> 0.86	< 1.21	< 65	< 63
$\Omega_M + \Omega_\Lambda = 1$	Corrected	> 0.77	< 1.27	< 83	< 78
	Uncorrected	> 0.75	< 1.30	< 78	< 70

Table 4.2: The 95% One-Tailed Confidence Levels for H_0^L/H_0^G

Bibliography

- [1] W. Baade. *ApJ*, 88:285, 1938.
- [2] J. G. Bartlett, A. Blanchard, J. Silk, and M. S. Turner. *Science*, 267:980, 1995.
- [3] M. S. Bessell. *PASP*, 102:1181, 1990.
- [4] M. S. Bessell. Private Communication, 1995.
- [5] M. Birkinshaw and J. P. Hughes. *ApJ*, 420:33, 1994.
- [6] M. Birkinshaw, J. P. Hughes, and K. A. Arnaud. *ApJ*, 379:466, 1991.
- [7] M. Bolte and C. J. Hogan. *Nature*, 376:399, 1995.
- [8] D. Branch. *ApJ*, 300:L51, 1986.
- [9] D. Branch, S.W. Falk, M.L. McCall, P. Rybski, A.K. Uomoto, and B.J. Wills.
ApJ, 270:123, 1983.
- [10] D. Branch and G. A. Tammann. *ARAA*, 30:359, 1992.

- [11] D. Branch, P. Nugent, A. Fisher In P. Ruiz-Lapuente, R. Canal, and J. Isern, editors, *Thermonuclear Supernovae*, Dordrecht, 1996, in press. Kluwer.
- [12] E. F. Bunn and N. Sugiyama. *ApJ*, 446:49, 1995.
- [13] D. Burstein and C. Heiles. *AJ*, 87:1165, 1982.
- [14] M. Capaccioli, E. Cappellaro, M. Della Valle, L. Rosino, and M. D'Onofrio. *ApJ*, 350:110, 1990.
- [15] J. A. Cardelli, G. C. Clayton, , and J. S. Mathis. *ApJ*, 345:235, 1989.
- [16] C. A. Christian, M. Adams, J. V. Barnes, H. Butcher, D. S. Hayes, J. R. Mould, and M. Siegel. *PASP*, 97:363, 1985.
- [17] C. J. Copi, D. N. Schramm, and M. S. Turner. *Science*, submitted; Fermilab-Pub-94/174-A, 1990.
- [18] A. W. J. Cousins. *memras*, 81:25, 1976.
- [19] H. Dahle, S. J. Maddox, and P. B. Lilje. *ApJ*, 435:79, 1994.
- [20] L. Davis. Private Communication, 1995.
- [21] G. de Vaucouleurs. *AJ*, 63:253, 1958.
- [22] L. A. Dreiling and R. A. Bell. *AJ*, 241:736, 1980.
- [23] A. Dressler, S. M. Faber, D. Burstein, R. L. Davies, and D. Lynden-Bell. *ApJ*, 313:37, 1987.

- [24] J. H. Elias, K. Mathews, G. Neugebauer, and S. E. Persson. *ApJ*, 296:379, 1985.
- [25] A. V. Filippenko, M. W. Richmond, D. Branch, C. M. Gaskell, W. Herbst, C. H. Ford, R. R. Treffers, T. Matheson, L. C. Ho, A. Dey, W. L. Sargent, T. A. Small, and W. J. M. van Breugel. *AJ*, 104:1543, 1992.
- [26] A. V. Filippenko, M. W. Richmond, T. Matheson, M. Dickinson, J. C. Shields, E. M. Burbidge, R. D. Cohen, B. Malkan, M. A. and Nelson, and J. Pietz. *ApJ*, 384:L15, 1992.
- [27] A. Fisher, D. Branch, P. Höflich, and A. Khokhlov. *ApJ*, 447:L73, 1995.
- [28] C. H. Ford, W. Herbst, M. W. Richmond, M. L. Baker, A. V. Filippenko, R. R. Treffers, Y. Paik, and P. J. Benson. *AJ*, 106:1101, 1993.
- [29] W. L. Freedman, B. F. Madore, J. R. Mould, R. Hill, L. Ferrarese, R. C. Kennicutt, A. Saha, P. B. Stetson, J. A. Graham, H. Ford, J. G. Hoessel, J. Huchra, S. M. Hughes, and G. D. Illingworth. *Nature*, 371:757, 1994.
- [30] G. Goldhaber, S. Deustua, S. Gabi, G. Goldhaber, D. Groom, I. Hook, A. Kim, M. Kim, J. Lee, C. Pain, R. Pennypacker, S. Perlmutter, I. Small, A. Goobar, R. Ellis, R. McMahon, B. Boyle, P. Bunclark, D. Carter, K. Glazebrook, M. Irwin, H. Newberg, A. V. Filippenko, T. Matheson, M. Dopita, J. Mould, and W. Couch. In *Thermonuclear Supernovae*. Dordrecht:Kluwer, 1996.
- [31] G. et al. Goldhaber. In preparation, 1996.

- [32] A. Goobar and S. Perlmutter. *ApJ*, 450:14, 1995.
- [33] J. E. Gunn. In A. Maeder, L. Martinet, and G. Tammann, editors, *Observational Cosmology : 8th advanced course of the Swiss Society of Astronomy and Astrophysics*, Sauverny, Geneva, 1978.
- [34] J. E. Gunn and L. L. Stryker. *ApJS*, 52:121, 1983.
- [35] M. Hamuy, M. M. Phillips, J. Maza, N. B. Suntzeff, R. A. Schommer, and R. Aviles. *AJ*, 109:1, 1995.
- [36] M. Hamuy, M. M. Phillips, R. A. Schommer, N. B. Suntzeff, and J. Maza. *AJ*, *in press*, 1996.
- [37] M. Hamuy, M. M. Phillips, L. A. Wells, and J. Maza. *PASP*, 105:787, 1993.
- [38] M. Hamuy, A. R. Walker, N. B. Suntzeff, P. Gigoux, S. R. Heathcote, and M. M. Phillips. *PASP*, 104:533, 1992.
- [39] R. P. Harkness, J. C. Wheeler, B. Margon, R. A. Downes, R. P. Kirshner, A. Uomoto, E. S. Barker, A. L. Cochran, H. L. Dinerstein, D. R. Garnett, and R. M. Levreault. *ApJ*, 317:355, 1987.
- [40] G. H. Jacoby, D. Branch, R. Clardullo, R. L. Davies, W. E. Harris, M. J. Pierce, C. J. Pritchett, J. L. Tonry, and D. L. Welch. *PASP*, 104:599, 1992.
- [41] M. Joeever. *Astrofizica*, 18:574, 1982.

- [42] H. L. Johnson. *Ann. Astrophys.*, 18:292, 1955.
- [43] H. L. Johnson and D. L. III Harris. *Apj*, 120:196, 1954.
- [44] H. L. Johnson and W. W. Morgan. *ApJ*, 117:313, 1953.
- [45] R. C. Kennicutt. *ApJS*, 79:255, 1992.
- [46] A. G. Kim, A. Goobar, and S. Perlmutter. *PASP*, 108:190, 1996.
- [47] A. Kim, S. Gabi, G. Goldhaber, D. Groom, I. Hook, M. Kim, J. Lee, S. Perlmutter, C. Pennypacker, I. Small, A. Goobar, R. Pain, R. Ellis, R. McMahon, B. Boyle, P. Bunclark, D. Carter, M. Irwin, K. Glazebrook, H. Newberg, A. V. Filippenko, T. Matheson, M. Dopita, and W. Couch. *In press*, 1996.
- [48] R.P. Kirshner and et al. *ApJ*, 415:589, 1993.
- [49] A. U. Landolt. *AJ*, 78:959, 1973.
- [50] A. U. Landolt. *AJ*, 88:439, 1983.
- [51] A. U. Landolt. *AJ*, 104:340, 1992.
- [52] T.R. Lauer and M. Postman. *ApJ*, 400:L47, 1992.
- [53] T.R. Lauer and M. Postman. *ApJ*, 425:L418, 1994.
- [54] B. Leibundgut. PhD thesis, University of Basel, 1988.
- [55] B. Leibundgut. *AAP*, 229:1, 1990.

- [56] B. Leibundgut, R.P. Kirshner, A.V. Filippenko, J.C. Shields, C.B. Foltz, M.M. Phillips, and G. Sonneborn. *ApJ*, 371:L23, 1991.
- [57] B. Leibundgut, G.A. Tammann, R. Cadonau, and D. Cerrito. *AApS*, 89:537, 1991.
- [58] D. Lynden-Bell, S. M. Faber, D. Burstein, R. L. Davies, and A. Dressler. *ApJ*, 326:L19, 1988.
- [59] S. N. Milford. *ApJ*, 122:13, 1955.
- [60] R. Minkowski. *ApJ*, 89:156, 1939.
- [61] R. Minkowski. *PASP*, 52:206, 1940.
- [62] K. Nomoto, F.-K. Thielemann, and K. Yokoi. *ApJ*, 286:644, 1984.
- [63] H. U. Nørgaard-Nielson, L. Hansen, H. E. Jørgensen, A. A. Salamanca, R. S. Ellis, and W. J. Couch. *Nature*, 339:523, 1989.
- [64] P. Nugent, M. Phillips, E. Baron, D. Branch, and P. Hauschildt. *ApJ*, 455:L147, 1995.
- [65] S. C. Odewahn, C. Bryja, and R. M. Humphreys. *PASP*, 104:553, 1992.
- [66] J. B. Oke and A. Sandage. *ApJ*, 154:21, 1968.
- [67] R. Pain, I. Hook, S. Deustua, S. Gabi, G. Goldhaber, D. Groom, A. Kim, M. Kim, J. Lee, C. Pennypacker, S. Perlmutter, I. Small, A. Goobar, R. Ellis,

- R. McMahon, K. Glazebrook, B. Boyle, P. Bunclark, D. Carter, and M. Irwin.
ApJ, In Press, 473, 1996.
- [68] P.J.E. Peebles. *Principles of Physical Cosmology*, page 330. Princeton University Press, Princeton, 1993.
- [69] S. Perlmutter, S. Deustua, S. Gabi, G. Goldhaber, D. Groom, I. Hook, A. Kim, M. Kim, J. Lee, C. Pain, R. Pennypacker, I. Small, A. Goobar, R. Ellis, R. McMahon, B. Boyle, P. Bunclark, D. Carter, K. Glazebrook, M. Irwin, H. Newberg, A. V. Filippenko, T. Matheson, M. Dopita, J. Mould, and W. Couch. In P. Ruiz-Lapuente, R. Canal, and J. Isern, editors, *Thermonuclear Supernovae*, Dordrecht, 1996, in press. Kluwer.
- [70] S. Perlmutter, S. Deustua, G. Goldhaber, D. Groom, I. Hook, A. Kim, M. Kim, J. Lee, J. Melbourne, C. Pennypacker, I. Small, A. Goobar, R. Pain, R. Ellis, R. McMahon, B. Boyle, P. Bunclark, D. Carter, M. Irwin, A. V. Filippenko, A. Barth, W. Couch, M. Dopita, J. Mould, and D. York. IAU Circ. No. 6270, 1995.
- [71] S. Perlmutter, S. Gabi, G. Goldhaber, D. Groom, I. Hook, A. Kim, M. Kim, J. Lee, C. Pennypacker, I. Small, A. Goobar, R. Pain, R. Ellis, R. McMahon, B. Boyle, P. Bunclark, D. Carter, M. Irwin, K. Glazebrook, H. Newberg, A. V. Filippenko, T. Matheson, M. Dopita, and W. Couch. *ApJ, accepted*, 1996.

- [72] S. Perlmutter, C. Pennypacker, G. Goldhaber, A. Goobar, R. Pain, B. Grossan, A. Kim, M. Kim, and I. Small. IAU Circ. Nos. 5956 and 5958, 1994.
- [73] S. Perlmutter, C. R. Pennypacker, G. Goldhaber, A. Goobar, R. A. Muller, H. J. M. Newberg, J. Desai, A. G. Kim, M. Y. Kim, I. A. Small, B. J. Boyle, C. S. Crawford, R. G. McMahon, P. S. Bunclark, D. Carter, M. J. Irwin, R. J. Terlevich, R. S. Ellis, K. Glazebrook, W. J. Couch, J. R. Mould, T. A. Small, and R. G. Abraham. *ApJ*, 440:L41, 1995.
- [74] S. Perlmutter et al. In preparation, 1996.
- [75] M. M. Phillips. *ApJ*, 413L:105, 1993.
- [76] M. M. Phillips, L. A. Wells, N.B. Suntzeff, M. Hamuy, B. Leibundgut, R.P. Kirshner, and C.B. Foltz. *AJ*, 103:1632, 1992.
- [77] M. J. Pierce, D. L. Welch, R. D. McClure, S. van den Bergh, R. Racine, and P. B. Stetson. *Nature*, 371:385, 1994.
- [78] A. C. Porter and A. V. Filippenko. *AJ*, 93:1372, 1987.
- [79] Yu. P. Pskovskii. *Astron Zh.*, 47:994, 1970.
- [80] Yu. P. Pskovskii. *Sov. Astron. AJ*, 21:675, 1977.
- [81] A. G. Riess, W. H. Press, and R. P. Kirshner. *ApJ*, 445:L91, 1995.
- [82] A. G. Riess, W. H. Press, and R. P. Kirshner. *ApJ*, 438:L17, 1995.

- [83] A. G. Riess, W. H. Press, and R. P. Kirshner. *ApJ*, *in press*, 1996.
- [84] B. W. Rust. PhD thesis, University of Illinois, 1974.
- [85] A. Saha, L. Labhardt, H. Schwengeler, F. D. Macchetto, N. Panagia, A. Sandage, and G. A. Tammann. *ApJ*, 425:14, 1994.
- [86] A. Saha, A. Sandage, L. Labhardt, H. Schwengeler, G. A. Tammann, N. Panagia, and F. D. Macchetto. *ApJ*, 438:8, 1995.
- [87] A. Sandage and J. Perelmuter. *ApJ*, 370:455, 1991.
- [88] A. Sandage, A. Saha, G. A. Tammann, L. Labhardt, N. Panagia, and F. D. Macchetto. *ApJ*, 460:L15, 1996.
- [89] D. P. Schneider, J. G. Hoessel, and J. E. Gunn. *ApJ*, 264:337, 1983.
- [90] N.B. Suntzeff. In preparation, 1995.
- [91] G. A. Tammann. In M. J. Rees and R. J. Stoneham, editors, *Supernovae: A Survey of Current Research*, page 371, Dordrecht, 1982. Reidel.
- [92] G. A. Tammann. In A. Hewitt, G. Burbidge, and L. Z. Fang, editors, *IAU Symposium 124, Observational Cosmology*, page 151, Dordrecht, 1987. Reidel.
- [93] G. A. Tammann and B. Leibundgut. *AAP*, 236:9, 1990.
- [94] N. R. Tanvir, T. Shanks, H. C. Ferguson, and D. R. T. Robinson. *Nature*, 377:27, 1995.

- [95] E.L. Turner, R. Cen, and J. P. Ostriker. *ApJ*, 103:1427, 1992.
- [96] S. van den Bergh and J. Pazder. *ApJ*, 390:34, 1992.
- [97] T. Vaughan, D. Branch, D. Miller, and S. Perlmutter. *ApJ*, 439:558, 1995.
- [98] T. Vaughan, D. Branch, and S. Perlmutter. *ApJ submitted*, 1995.
- [99] O. C. Wilson. *ApJ*, 90:634, 1939.
- [100] X. Wu, B. Qin, and L. Fang. *ApJ, in press*, 1996.
- [101] K. Yamashita. In F. Makino and T. Ohashi, editors, *New Horizon of X-ray Astronomy - First Results from ASCA*, page 279, Tokyo, 1994. Universal Academy Press.

M98052837



Report Number (14) LBNL -- 40840

Publ. Date (11) 199709
Sponsor Code (18) DOE/ER, XF
JC Category (19) KC-412, DOE/ER

DOE